Multiple roles for the ESCRT machinery in maintaining plasma membrane homeostasis

Oliver Schmidt[1*], Yannick Weyer[1], Simon Sprenger[1], Michael A. Widerin[1], Sebastian Eising[2], Verena Baumann[1,3], Mihaela Angelova[4], Robbie Loewith[5], Christopher J. Stefan[6], Michael W. Hess[7], Florian Fröhlich[3], and David Teis[1]

[1] Institute for Cell Biology, Biocenter, Medical University of Innsbruck, Austria
[2] Department of Biology/Chemistry, University of Osnabrück, Germany
[3] current address: Max Perutz Labs, University of Vienna, Austria
[4] Cancer Evolution and Genome Instability Laboratory, Francis Crick Institute, London, UK
[5] Department of Molecular Biology, University of Geneva, Switzerland
[6] MRC Laboratory for Molecular Cell Biology, University College London, London, UK
[7] Institute for Histology and Embryology, Medical University of Innsbruck, Austria

*Corresponding author:
Dr. Oliver Schmidt
Medical University of Innsbruck, Biocenter, Division Cell Biology
Innrain 80/82, CCB Building
A-6020, Innsbruck, Austria

oliver.schmidt@i-med.ac.at
phone: +43 512 9003 70191
fax: +43 512 9003 73100

Running title: The ESCRT machinery and membrane homeostasis

ABSTRACT

The endosomal sorting complexes required for transport (ESCRT) execute evolutionary conserved membrane remodeling processes. Here we used budding yeast to explore how the ESCRT machinery contributes to plasma membrane (PM) homeostasis. In response to reduced membrane tension and inhibition of the target of rapamycin complex 2 (TORC2), ESCRT-III/Vps4 assemblies form at the PM and help to maintain membrane integrity. Conversely, the growth of ESCRT mutants strongly depends on TORC2-mediated homeostatic regulation of sphingolipid (SL) metabolism. This is caused by calcineurin phosphatase activity which causes Orm2 to accumulate at the endoplasmic reticulum (ER) in ESCRT mutants. Orm2 is a repressor of SL biosynthesis and its accumulation provokes increased membrane stress. This necessitates TORC2 signaling through its downstream kinase Ypk1 to control Orm2 protein levels and prevent a detrimental imbalance of SL metabolism. Our findings reveal new aspects of antagonistic calcineurin/TORC2 signaling for the regulation of SL biosynthesis and the maintenance of PM homeostasis, and suggest that the ESCRT machinery contributes directly and indirectly to these processes.

Key words: sphingolipid / membrane / stress / Endosomal sorting complexes required for transport (ESCRT) / mTOR complex (mTORC) / calcineurin / membrane stress / TORC2 / ORMDL family / Endosome and Golgi-associated degradation (EGAD)

Introduction

Eukaryotic cells harmonize lipid homeostasis and protein homeostasis (proteostasis) to maintain the integrity of their membranes. This requires the balanced synthesis of proteins and lipids and their selective degradation. How these processes are coordinated is only partially understood.

Selective membrane protein degradation is mediated through several ubiquitin-dependent degradation pathways. In the ER, the multi-subunit transmembrane ubiquitin ligases of the ER-associated degradation (ERAD) machinery ubiquitinate membrane proteins for retro-translocation into the cytoplasm and subsequent proteasomal degradation (1,2). ERAD can also degrade functional proteins in a regulated manner and thereby control membrane homeostasis. An important regulated ERAD substrate is the 3-hydroxy-3-methylglutaryl coenzyme A reductase (HMGR), a key enzyme in sterol biosynthesis (3,4). HMGR degradation is part of a rheostat that is critical for sterol homeostasis in yeast and humans. Also, squalene monooxygenase is subject to sterol-regulated ERAD (5,6). When the folding and degradation capacity of the ER and ERAD are overwhelmed, mis-folded proteins accumulate and induce a cellular stress response pathway, called the unfolded protein response (UPR). The UPR implements adaptive transcriptional programs that resolve ER stress by a decrease in overall protein synthesis and a specific up-regulation of hundreds of genes including lipid biosynthesis, ER chaperons and ERAD machineries (7). Consistently, simultaneous loss of ERAD and UPR decreases viability of yeast cells (8).

Proteins in post-ER organelles are degraded by different degradation pathways. We recently described the endosome and Golgi-associated degradation (EGAD) pathway (9). EGAD is mediated by the defective in sterol-responsive element binding protein (SREBP) cleavage (Dsc) complex, a multi-subunit transmembrane ubiquitin ligase reminiscent of the complexes operating in ERAD (10). During EGAD, the Dsc complex ubiquitinates membrane proteins at the Golgi and endosomes and thereby initiates their extraction into the cytosol by the AAA (ATPase associated with diverse cellular activities) protein Cdc48, which leads to their proteasomal degradation (9). The Dsc complex also ubiquitinates a distinct set of substrates for lysosomal degradation via the ESCRT machinery (discussed below) (11-14). The EGAD and ESCRT machineries show a strong negative genetic interaction (synthetic growth defect), suggesting that they have non-redundant functions and non-overlapping substrates (9,14).

A substrate that is exclusively degraded via the EGAD pathway is the transmembrane protein Orm2 (9). Orm2 and its paralog Orm1 are critical components of the multi-subunit SPOTS complex in the ER. The SPOTS complex consists of Orm1/2, the catalytic subunits of the serine-palmitoyl-coenzyme A transferase (SPT, Lcb1 and Lcb2) and of the regulatory factors Tsc3 and Sac1 (15,16). The SPT mediates sphingoid long chain base (LCB) synthesis and is rate limiting for sphingolipid metabolism. The Orm1/2 proteins repress SPT activity and ensure that the SPT only produces LCBs that are subsequently consumed in SL biosynthesis. Thereby Orm1/2 prevent the toxic accumulation of LCBs. The function of Orm1/2 is evolutionary conserved. Loss of ORMDL1-3, their mammalian orthologues, results in neurotoxicity in mice (17), whereas increased expression of ORMDL3 causes imbalances in sphingolipid metabolism in humans, and is associated with childhood asthma, Crohn's disease, ulcerative colitis and diabetes (18-21). In yeast, the de-repression of SPT activity is mediated by phosphorylation of the Orm1/2 proteins in their N-terminal cytosolic domain by the AGC-family serine-threonine protein kinase Ypk1 (22). Phosphorylated Orm2 is exported from the ER to Golgi and endosomes, where the protein is degraded by the EGAD machinery (9).

Ypk1, the yeast orthologue of the mammalian serum- and glucocorticoid-induced protein kinase SGK1, is activated through phosphorylation by two upstream kinases. Phosphorylation of the activation loop by phosphoinositide-dependent kinase (Pkh1/2 in yeast) is essential for activity, but full activation requires phosphorylation from the target of rapamycin complex 2 (TORC2) (23). In yeast, TORC2 is an essential, PM-localized multi-subunit protein kinase whose activity responds to membrane stress conditions such as changes in PM tension (24,25) and sphingolipid levels (26). How TORC2 senses membrane stress is largely unknown, but its regulation involves the dynamic partitioning of TORC2 subunits into membrane subdomains which can either promote (24,27) or inhibit (25) activity. In addition TORC2 can be regulated by association with Rab5-family proteins (28). Activation of Ypk1 by TORC2 requires its regulated recruitment to the plasma membrane by the TORC2 accessory proteins Slm1/2 (24,29) and the TORC2 subunit Avo1 (30). The phosphorylation of the Orm1/2 proteins constitutes the essential function of the TORC2-Ypk1 signaling axis (22,31). Further Ypk1-regulated processes include the stimulation of ceramide synthesis (32), aminophospholipid transport (33), osmoregulation (34,35) and endocytosis/actin cytoskeleton dynamics (31,36-38), all impinging in one way or another on membrane homeostasis. Ypk1 has a paralogue, Ypk2, which shares its activation by Pkh1/2 and TORC2. Ypk1 and Ypk2 are believed to share

123 a largely overlapping substrate spectrum. Since the simultaneous deletion of both kinases is
124 lethal, Ypk1 and Ypk2 at least partially compensate for each other's function (39). However,
125 only Ypk1 activity is required for normal growth of yeast cells.
126
127 The degradation of most membrane proteins of the PM, the Golgi or endo- and lysosomal
128 membranes occurs inside lysosomes (vacuoles in yeast) and depends on the ESCRT machinery
129 (40-43). Early ESCRT complexes (ESCRT-0, -I, -II) probably cluster and sequester
130 ubiquitinated cargo proteins on the endosome surface and initiate the formation of the
131 filamentous ESCRT-III complex. Dynamic remodeling of the ESCRT-III complex by the AAA
132 ATPase Vps4 and its partner proteins drives the budding of small cargo-laden vesicles into the
133 lumen of the endosome (44). This process generates multivesicular bodies (MVB), which
134 subsequently fuse with the lysosome/vacuole. Some cargo proteins are also budded by the
135 ESCRT machinery directly from the lysosomal surface into the lumen in response to TORC1
136 inactivation (45-47). Loss of function of the ESCRT machinery leads to the formation of
137 aberrant, peri-vacuolar endosomal structures called class E compartments, where substrates of
138 the MVB pathway accumulate (48). The ESCRT machinery is additionally involved in many
139 other cellular membrane remodeling events, including abscission of the midbody at the end of
140 cytokinesis, the generation of exosomes, or budding of enveloped viruses (e.g. HIV) (for a
141 recent review on ESCRT functions, see (41,49)). The ESCRT machinery also repairs ruptured
142 lysosomal, nuclear and plasma membranes (50-58).
143
144 While regulatory roles of ERAD and EGAD in lipid metabolism have been described, it is less
145 clear how the ESCRT machinery contributes to membrane homeostasis. Here we show that the
146 ESCRT machinery has an essential and complex role in maintaining PM homeostasis. ESCRT-
147 III/Vps4 assemblies form at the PM in response to reduced PM tension or TORC2 inhibition.
148 Cells without a functional ESCRT machinery are hyper-sensitive to plasma membrane stress
149 conditions and require TORC2-Ypk1 signaling to maintain PM integrity and promote growth
150 and survival. The mutual dependence of the ESCRT machinery and TORC2-Ypk1 signaling is
151 caused by accumulation of Orm2 at the ER. In ESCRT mutants, Orm2 is not efficiently
152 exported from the ER because the phosphatase calcineurin counteracts Orm2 ER export by
153 causing its untimely dephosphorylation. The accumulating Orm2 proteins at the ER trigger
154 elevated TORC2-Ypk1 signaling to maintain homeostasis, and loss of Ypk1 signaling in
155 ESCRT mutants results in a fatal imbalance in SL metabolism with an accumulation of LCBs.
156 Importantly, preventing calcineurin-dependent Orm2 dephosphorylation promoted the

157 degradation of Orm2 by EGAD, and was sufficient to break the dependence of ESCRT mutants
158 on TORC2-Ypk1 signaling. This demonstrates that the accumulation of Orm2 at the ER is a
159 major membrane stressor. Moreover, our results reveal an important link between selective
160 membrane protein degradation systems in post-ER compartments and TORC2-Ypk1 dependent
161 membrane stress signaling.

162 **Results**

163

164 **ESCRT mutants depend on TORC2-Ypk1 signaling for cell growth and survival**

165 The evolutionary conserved ESCRT complexes assemble into membrane remodeling
166 machineries that execute fundamental biological processes, including the biogenesis of
167 multivesicular bodies for lysosomal membrane protein degradation and the repair of diverse
168 cellular membranes (41). Given these key roles of the ESCRT machinery, it is surprising that
169 ESCRT mutant cells are viable. This implies that cells can at least in part compensate for the
170 loss of ESCRT function. Understanding how cells achieve this compensation would therefore
171 also provide a better understanding for the role of the ESCRT machinery in cellular homeostatic
172 processes.

173

174 To identify the processes that enable the survival of ESCRT-deficient cells, we used the
175 budding yeast, *S. cerevisiae*, as a model system and conducted a genome-wide synthetic genetic
176 interaction screen (9). Gene ontology (GO) term enrichment analysis revealed 'lipid
177 metabolism' among the top ranked hits that are required by ESCRT mutants (*vps4*Δ) (Fig. 1A,
178 Table S1). This GO term included genes involved in the metabolism of various lipid classes,
179 but predominantly enzymes mediating non-essential steps of sterol biosynthesis, and genes
180 regulating SL homeostasis. We confirmed the synthetic growth defect of *vps4*Δ cells with four
181 of these genes (*ypk1*Δ, *sac1*Δ, *csg2*Δ, *erg2*Δ) in a different genetic background (the SEY6210
182 strain) (Fig. S1A). These results suggested that the loss of ESCRT-dependent membrane
183 remodeling rendered cells particularly sensitive to perturbations of membrane homeostasis.

184

185 We focused on the role of the protein kinase Ypk1 in ESCRT-deficient cells, because it
186 functions together with TORC2 to maintain membrane homeostasis (22,24,33,36,59,60). *YPK1*
187 deletion (but not deletion of *YPK2*) also caused synthetic growth defects with ESCRT-II
188 (*vps25*Δ) and ESCRT-III mutants (*vps2*Δ), but not with mutants of Chm7 (*chm7*Δ)(Fig. S1B),
189 which recruits the ESCRT machinery to the ER and the inner nuclear membrane (51,52,61).
190 This result suggested that the function of Ypk1 was required to compensate for the loss of
191 ESCRT functions that are independent of Chm7.

192

193 The growth of *vps4*Δ *ypk1*Δ double mutants was restored by re-expression of *VPS4* and *YPK1*
194 from plasmids (Fig. S1C), but not by an additional copy of *YPK2* (39,62). Expression of a Ypk1
195 mutant (Ypk1 S644A, T662A) that can no longer be activated by TORC2 failed to rescue the

196 growth of *vps4*Δ *ypk1*Δ (Fig. 1B,C) or *vps2*Δ *ypk1*Δ (Fig. S1D) double mutants, similar to the
197 catalytically dead T504A mutant (63). The constitutively active D242A mutant (22) restored
198 normal growth of the double mutants, even when the TORC2 acceptor sites were mutated (Fig.
199 1B, S1D). Hence, TORC2-dependent Ypk1 activation was required in ESCRT mutants.
200
201 To further characterize the relation between TORC2 signaling and the ESCRT machinery, we
202 analyzed the growth of WT and ESCRT mutant cells, which were genetically engineered for
203 the selective inhibition of TORC2 (*tor1-1 AVO3*$^{\Delta 1274\text{-}1430}$) with rapamycin (64). At 2 nM
204 rapamycin the growth of WT cells was only mildly affected (64), but the growth of *vps4*Δ
205 mutants was already markedly reduced (Fig. 1D).
206
207 TORC2 responds to perturbation of the PM, and acute reduction of PM tension with palmitoyl-
208 carnitine (PalmC) leads to transient TORC2 inactivation (25). Importantly, the growth of WT
209 cells was not affected by low doses of PalmC (5 µM), suggesting that they were capable to
210 maintain homeostasis. Yet, the same PalmC concentration already slowed down the growth of
211 *vps4*Δ or *vps2*Δ cells (Fig. 1E), suggesting that ESCRT function somehow contributed to
212 viability upon PM stress.
213
214 Thus, our results imply that TORC2-Ypk1 signaling and the ESCRT machinery have non-
215 redundant functions that together are critical to maintain membrane homeostasis and promote
216 growth.
217
218 **ESCRT-III and Vps4 localize to plasma membrane structures upon TORC2 inhibition.**
219
220 TORC2 signaling responds to tensile stress at the PM and in consequence controls sphingolipid
221 synthesis and other processes to maintain PM homeostasis (24,25,65). How the ESCRT
222 machinery contributes to maintaining PM homeostasis was less clear. In human cells, the
223 ESCRT machinery localizes to PM lesions and repairs the ruptured areas, and also prolongs
224 PM integrity during necroptosis (56,66-68). If and how these processes might be correlated to
225 tensile PM stress and TORC2 signaling in budding yeast is unknown.
226
227 We therefore analyzed the localization of the major ESCRT-III subunit Snf7 in cells that were
228 treated with 5µM PalmC, a concentration that did not affect the growth of WT cells (Fig. 1E).
229 In untreated cells, Snf7-eGFP was mainly detected in the cytosol and on objects corresponding

230 to endosomes and multivesicular bodies (MVBs) (44) (Fig. 2A, arrowheads). Upon addition of
231 PalmC, we detected the formation of additional Snf7-eGFP foci at or close to the PM (Fig. 2A,
232 arrows). After 2 hours, at least three of these structures were observed in the majority of cells
233 (66%) (Fig. 2A, B). Thus, ESCRT-III assemblies formed at the PM in response to PalmC-
234 induced membrane perturbations.
235
236 Next, we tested if the localization of ESCRT-III to the PM was a consequence of TORC2
237 inactivation. We determined the localization of Snf7 and of the AAA-ATPase Vps4 upon
238 sublethal inhibition of TORC2 signaling (2 nM rapamycin) (Fig. 1D). Similar to the PalmC-
239 treated cells, Snf7-eGFP and Vps4-eGFP assemblies formed at the PM in many cells (> 75%)
240 after 2 hours of TORC2 inhibition (Fig. 2B, C, arrows). One or two sub-cortical Snf7-eGFP
241 and Vps4-eGFP dots but rarely more were also observed in control WT cells (in 22-34% of
242 cells) (Fig. 2B).
243
244 To describe the identity of the Snf7-eGFP positive structures that emerge upon PM stress at the
245 ultrastructural level, we performed cryofixation and immunogold electron microscopy (44).
246 After 60 min of sublethal TORC2 inhibition, we observed numerous vesicular structures at or
247 near the PM (Fig. 2D). PM-associated vesicles likely represented invaginations, possibly
248 reflecting stalled endocytic events, since TORC2 signaling stimulates endocytosis on multiple
249 levels (31,36,65). Snf7-eGFP localized to these invaginations (Fig. 2D (i)), to extended tubular
250 invaginations (ii) as well as to flat areas and vesicular structures in close vicinity to the PM (iii).
251
252 The localization of Snf7-eGFP to PM foci in response to PalmC treatment or direct TORC2
253 inhibition required the activity of Vps4. In *vps4*Δ mutants, Snf7-eGFP remained associated with
254 class E compartments (44) (Fig. 2A, B, C). Of note, the growth of *vps4*Δ cells was already
255 severely affected under these conditions (Fig.1D, E) suggesting that the localization of ESCRT-
256 III/Vps4 to the PM might help to mitigate PM stress and prevent cell injuries.
257
258 Chronic inactivation of Ypk1 (chronic TORC2 inactivation is lethal) in *vps4*Δ mutants
259 dramatically increased the frequency of PM integrity defects. This was assessed using
260 propidium iodide (PI) staining. PI is membrane impermeable and only enters yeast cells when
261 the integrity of the PM is corrupted. In WT cells, but also in *vps4*Δ and *ypk1*Δ single mutants
262 the frequency of PI positive cells was low (Fig. 2E). However, the frequency of PI positive cells

263 strongly increased in *vps4*Δ *ypk1*Δ double mutants (Fig. 2E), suggesting that they failed to
264 maintain PM integrity.
265
266 These results demonstrated that TORC2-Ypk1 signaling and the ESCRT machinery helped to
267 maintain the integrity of the PM. In response to acute PM stress the formation of ESCRT-
268 III/Vps4 assemblies at the PM promoted cell survival. Chronic loss of Ypk1 signaling and the
269 inability to form ESCRT-III/Vps4 assemblies at the PM compromised membrane integrity. This
270 might be the leading cause for their synthetic genetic interaction and the mutual dependence of
271 ESCRT function and TORC2-Ypk1 signaling
272
273 **TORC2-Ypk1 signaling prevents detrimental SL imbalance in ESCRT mutants**
274
275 Next, we addressed how TORC2-Ypk1 signaling and the function of the ESCRT machinery
276 converge to mitigate membrane stress. Therefore, we first defined the molecular nature of
277 membrane stress in ESCRT mutants that is controlled by TORC2-Ypk1 signaling. Ypk1 is
278 activated by TORC2 through phosphorylation primarily of Ser 644 and Thr 662 (Fig. 1C)
279 (23,69). Importantly, ESCRT mutants not only had slightly higher steady state Ypk1 protein
280 levels, but also higher levels of active Ypk1 phosphorylated on Thr 662 (pT662) (Fig. 3A, Fig.
281 S3A, B). We found no evidence for ESCRT-dependent lysosomal turnover of Ypk1 (70) in
282 growing cells (Fig. S3C, D). The Ypk1 activation level in ESCRT mutants was substantial, but
283 still lower compared to the hyperactivation of TORC2 signaling upon treatment with the SPT
284 inhibitor myriocin (Fig. 3A, lane 1). Of note myriocin treatment for 150 min also reproducibly
285 resulted in the up-regulation of Ypk1 protein levels (Fig. 3A, lane 1). The elevated Ypk1 protein
286 levels that were detected in ESCRT mutants and in response to myriocin treatment might thus
287 reflect Ypk1 stabilization by TORC2 phosphorylation as described earlier (69). We also
288 observed a slight increase of *YPK1* mRNA in *vps4*Δ cells (Fig. S3E).
289
290 Ypk1 has a range of different cellular targets (31,32,59). Among those, the paralogous ER
291 proteins Orm1 and Orm2 are the essential targets of TORC2-Ypk1 (22,31). In ESCRT mutant
292 cells Orm2 protein levels and its Ypk1-dependent phosphorylation were increased (Fig. 3B).
293 Deletion of *YPK1* reduced but did not completely abrogate steady state phosphorylation of
294 Orm2 (presumably due to the presence of Ypk2), and caused upregulation of Orm2 protein
295 levels (Fig. 3B). In *vps4*Δ *ypk1*Δ double mutants Orm2 protein levels were higher than in either
296 single mutant.

297

298 TORC2-Ypk1 dependent phosphorylation of Orm2 and its paralogue Orm1 is required to de-
299 repress the synthesis of LCBs by the SPT complex (15,22) (Fig. 3C). TORC2 and Ypk1 also
300 stimulate a subsequent step in the SL biosynthetic pathway by phosphorylating Lag1 and Lac1,
301 two components of the ER-resident ceramide synthase (CS) (71,72) (Fig. 3C). This concerted
302 regulation avoids the toxic accumulation of biosynthetic intermediates and helps to maintain
303 SL homeostasis (32).
304

305 We assessed the steady state levels of LCBs and ceramides using liquid chromatography - mass
306 spectrometry (LC-MS) analysis. Despite the accumulation of Orm2 in *vps4*Δ cells, total LCBs
307 (C18-PHS and C18-DHS) and ceramides were not lower than in WT cells (Fig. 3D). Also *in*
308 *vivo* labeling of the SL pool with [^{3}H]-L-serine in WT cells and *vps4*Δ cells showed only subtle
309 differences in the steady state levels of mannosylated SL species, but the overall formation of
310 [^{3}H]-labelled complex SL was comparable (Fig. 3E). It seemed that steady state levels of SL
311 synthesis in ESCRT mutants were maintained by Ypk1-dependent phosphorylation of Orm2.
312 Consistently, loss of Ypk1 in *vps4*Δ mutants skewed SL biosynthesis. In *vps4*Δ *ypk1*Δ double
313 mutants, the steady state LCB levels were increased (> 3-fold), while ceramide levels remained
314 similar to *vps4*Δ single mutants (Fig. 3D). The loss of Ypk1 signaling in ESCRT mutants
315 apparently caused an imbalance of SPT and CS activity, implying that the activity of CS might
316 have become a bottleneck. Consistently, we observed that *vps4*Δ *ypk1*Δ double mutants
317 produced less complex SL (predominantly inositolphosphoryl-ceramide (IPC)) than both WT
318 and *vps4*Δ cells (Fig. 3E). Expression of a phospho-mimetic variant of CS can promote the
319 formation of ceramides and complex SL independently of Ypk1 activity (32). Indeed, ectopic
320 expression of the *LAG1*-S23,24E allele, which mimics constitutive Ypk1 phosphorylation (32),
321 partially restored the growth of *vps4*Δ *ypk1*Δ cells (Fig. 3F).
322

323 These results demonstrate that ESCRT mutants have elevated Orm2 protein levels. TORC2-
324 Ypk1 signaling partially compensates for the defects ensuing from Orm2 accumulation.
325 Therefore, the SL profile of ESCRT mutants shows rather subtle differences compared to WT
326 cells. Consistent with this notion, the deletion of *YPK1* in ESCRT mutants caused a detrimental
327 imbalance in SPT and CS activity, characterized by an accumulation of LCBs and an impaired
328 conversion into ceramides and complex SL. This imbalance in SL homeostasis might contribute
329 to the defects in PM integrity observed in *vps4*Δ *ypk1*Δ mutants.
330

331 **In ESCRT mutants Orm2 is retained in the ER**

332

333 While Orm2 protein levels were up-regulated in ESCRT mutants, the protein levels of Orm1 or
334 other subunits of the SPOTS complex were unaffected (Fig. S4A). The changes in *ORM2*
335 mRNA levels were minor and similar to *ORM1* (Fig. S4B), and cannot explain the increase of
336 Orm2 protein. We concluded that the increase in Orm2 protein levels was caused by selective
337 post-transcriptional mechanisms. The protein levels of Orm2 (but not Orm1) are controlled by
338 a multistep process that delivers Orm2 from the ER to EGAD. First Orm2 is phosphorylated on
339 Ser 46,47,48 by Ypk1. Next, phosphorylated Orm2 is exported from the ER in a COP-II-
340 dependent manner. Once Orm2 arrives at the Golgi and on endosomes, it is recognized and
341 ubiquitinated by the Dsc ubiquitin ligase complex, which ensures its proteasomal degradation
342 (9).

343

344 To understand which of these steps are affected in ESCRT mutants, we compared them to
345 EGAD mutants. Orm2 protein levels and its phosphorylation were similar in ESCRT (*vps4*Δ)
346 and EGAD (*tul1*Δ) mutants (Fig. 4A). However, Orm2 accumulated in different subcellular
347 compartments. In *tul1*Δ mutants GFP-Orm2 accumulated at the ER and on post-ER
348 compartments, including Golgi, endosomes and the vacuolar limiting membrane, as reported
349 earlier (9). In contrast, in the majority of *vps4*Δ cells, GFP-Orm2 was detected almost
350 exclusively at the ER (Fig. 4B). Only in some cells, we observed a partial colocalization of
351 GFP-Orm2 with the ESCRT substrate mCherry-CPS in class E compartments (Fig. S4C). Thus,
352 it seemed that in ESCRT mutants Orm2 accumulated mainly at the ER.

353

354 Consistent with earlier reports (73), we detected Tul1 and Ubx3, two essential components of
355 the Dsc complex, at the class E compartment in ESCRT mutants (Fig. S4D). Hence, the Dsc
356 complex could degrade Orm2 once it reached the class E compartment. Indeed, GFP-Orm2
357 strongly accumulated in class E compartments when the EGAD pathway was additionally
358 compromised in *vps4*Δ *tul1*Δ cells (Fig. 4B), in agreement with our earlier findings (9). The
359 mutant Orm2-K25,33R, which is no longer ubiquitinated by the Dsc complex and hence no
360 longer degraded, was also found predominantly in class E compartments in ESCRT mutants
361 (Fig. S4E). Native immunoprecipitation (IP) of Flag-Orm2 demonstrated that a fraction of
362 Orm2 still physically interacted with the Dsc complex in *vps4*Δ mutants (Fig. 4C), and
363 denaturing IP of Flag-Orm2 showed that it was ubiquitinated (Fig. 4D), although to a lower
364 extent compared to WT cells.

365

366 Consistently, Orm2 was still degraded in *vps4*Δ and *vps25*Δ mutants in cycloheximide chases,
367 although the half-life was substantially longer (Fig. 4E). In WT cells Orm2 was degraded with
368 a half-life of approximately 90 minutes, and in *vps4*Δ mutants the half-life of Orm2 was
369 approximately 180 minutes (Fig. 4E, F). In contrast, Orm2 degradation was fully blocked in
370 mutants of the Dsc complex (*tul1*Δ) (9) (Fig. 4E, F).

371

372 Collectively, these results support the idea that the ER export of Orm2 is reduced in ESCRT
373 mutants and causes accumulation of Orm2, despite a functional EGAD machinery.

374

375 **ER accumulation of Orm2 is caused by calcineurin and renders ESCRT mutants addicted**
376 **to TORC2-Ypk1 signaling**

377

378 Our results so far present a conundrum: In ESCRT mutants Orm2 is phosphorylated by TORC2-
379 Ypk1 (Fig. 3B, Fig. 4A), but still accumulates at the ER. Mutation of Ser 46,47,48 to alanine
380 in Orm2 (Orm2-3A) prevented phosphorylation by Ypk1 (22), reduced Orm2 ER export and
381 subsequent EGAD (9), and therefore Orm2-3A accumulated in WT cells and in *vps4*Δ mutants
382 (Fig. 5A). We also reported earlier that Ser 46,47,48 to aspartic acid mutations (Orm2-3D)
383 mimic constitutive phosphorylation and trigger constitutive ER export, leading to degradation
384 via EGAD. Therefore, Orm2-3D protein levels are low in WT cells. Importantly also in *vps4*Δ
385 mutants, Orm2-3D protein levels were strongly reduced (Fig. 5A). This result implied that in
386 *vps4*Δ mutants the phospho-mimetic Orm2-3D mutant could be exported more efficiently from
387 the ER, and then was degraded by EGAD. Remarkably, expression of the Orm2-3D mutant,
388 but not Orm2-3A, improved also the growth of *vps4*Δ *ypk1*Δ cells (Fig. 5B).

389

390 Since mimicking of constitutive phosphorylation improved Orm2 ER export and degradation
391 in ESCRT mutants, we can rule out general defects in ER export machineries or Orm2
392 degradation. Rather, these results implied that untimely dephosphorylation might hamper ER
393 export of Orm2. The calcium-dependent protein phosphatase calcineurin is a major antagonist
394 of TORC2 signaling (74), with regulatory roles in sphingolipid biosynthesis (26,32,60).
395 Moreover, membrane stress during heat shock has been linked to a mis-regulation of calcium
396 dynamics and calcineurin signaling impairing sphingolipid synthesis in the ER (60). ESCRT
397 mutant cells have been reported to be prone to accumulate intra-cellular calcium (75), with
398 increased activity of a calcineurin-dependent transcriptional reporter (76). Therefore, we

399 hypothesized that calcineurin activity in ESCRT mutants could counteract TORC2-Ypk1
400 signaling and thereby delay ER export and degradation of Orm2.
401
402 To test this hypothesis, we first acutely inhibited calcineurin with FK-506. Inhibition of
403 calcineurin for 30 minutes resulted in hyper-phosphorylation of Orm2 (Fig. 5C). It had been
404 shown before that calcineurin inhibition does not augment Ypk1 activation by TORC2 or
405 Pkh1/2 (22,24,32). Hyper-phosphorylation of Orm2 in response to calcineurin inhibition
406 suggested that this phosphatase was involved in the dephosphorylation of Orm2. Next, we
407 deleted the regulatory calcineurin subunit Cnb1, which chronically abrogates calcineurin
408 activity (77). Chronic loss of calcineurin activity in *cnb1*Δ cells also caused hyper-
409 phosphorylation of Orm2 and additionally led to slightly lower Orm2 protein levels compared
410 to WT cells. In *vps4*Δ mutants, deletion of *CNB1* markedly decreased Orm2 to levels that were
411 similar to WT cells (Fig. 5D). Thus, calcineurin activity results either directly or indirectly in
412 the dephosphorylation of Orm2, and thereby antagonizes TORC2-Ypk1-induced ER export and
413 degradation of Orm2.
414
415 Calcineurin activity also rendered ESCRT mutants dependent on TORC2-Ypk1 signaling, since
416 deletion of *CNB1* partially restored the growth of *vps4*Δ *ypk1*Δ mutants (Fig. 5E). Likewise,
417 pharmacological inhibition of calcineurin activity (2µg/ml FK-506) or addition of the calcium-
418 chelator EGTA to the growth medium improved growth of *vps4*Δ *ypk1*Δ cells (Fig. 5F).
419 Calcineurin inhibition with FK-506 markedly decreased Orm2 protein levels in the *vps4*Δ
420 *ypk1*Δ double mutants (Fig. 5G). The inhibitory function of calcineurin was likely independent
421 of the transcription factor Crz1 which is a major downstream effector of calcineurin (78,79).
422 Unlike the deletion of *CNB1*, deletion of *CRZ1* did not rescue growth of *vps4*Δ *ypk1*Δ cells
423 (Fig. S5A). This is consistent with a role of calcineurin in controlling either directly or indirectly
424 Orm2 phosphorylation. Thus, calcineurin activity in ESCRT mutants reduced the ER export
425 and degradation of Orm2, which contributed to accumulation of Orm2 in the ER and rendered
426 the growth of ESCRT mutants dependent on TORC2-Ypk1 signaling.
427
428 Clearly, the accumulation of Orm2 constituted a major membrane stress factor in ESCRT
429 mutants: In *vps4*Δ *orm2*Δ double mutants Ypk1 activation by TORC2 (pT662) was no longer
430 elevated (Fig. 5G). In addition, *vps4*Δ *orm2*Δ cells grew better in presence of PalmC than *vps4*Δ
431 single mutants, suggesting a decreased susceptibility to PM stress (Fig. S5B). Furthermore,
432 deletion of *ORM2* in *vps4*Δ *ypk1*Δ double mutants restored membrane integrity and decreased

433 the fraction of PI-positive cells to *orm2*Δ single mutant levels (Fig S5C). Finally, the deletion
434 of *ORM2* fully rescued the growth defect of *vps4*Δ *ypk1*Δ cells (Fig. 5H). A partial rescue was
435 also observed upon deletion of *ORM1*.
436
437 Our results suggest that calcineurin activity in ESCRT mutant cells hampered the homeostatic
438 regulation of Orm2 ER export. In turn, Orm2 accumulated at the ER and was no longer
439 efficiently degraded by EGAD. The accumulation of Orm2 at the ER renders the growth of
440 ESCRT mutants dependent on TORC2-Ypk1 signaling to prevent imbalance in SL homeostasis
441 and loss of plasma membrane integrity (Fig. S5D).
442
443
444

445 **Discussion**

446

447 Here we show that the ESCRT machinery contributes directly and indirectly to PM homeostasis
448 in budding yeast and thereby takes part in ER-PM crosstalk to preserve the barrier function of
449 the PM.

450

451 ESCRT-III/Vps4 assemblies that form at the plasma membrane might play a direct role in
452 maintaining membrane integrity. A role for ESCRT complexes in repairing damaged PM was
453 described in human cells (56,66-68). There, injury-triggered calcium increase results in
454 assembly of ESCRT-III and accessory proteins at the site of repair via Alix (68). Yet, it is
455 unclear if ESCRTs also prevents membrane lesions in the first place. We observed ESCRT
456 assemblies at the PM in response to indirect (i.e by reduction of membrane tension) and direct
457 TORC2 inhibition. The major ESCRT-III subunit Snf7 and the AAA-ATPase Vps4 were
458 detected at PM invaginations and subcortical foci, which are reminiscent of stalled endocytic
459 buds. This seems plausible, since TORC2 promotes endocytosis by controlling actin and
460 endocytic proteins and by modulating membrane tension (31,36,65).

461

462 How ESCRT-III was recruited to these structures is currently unclear, but several scenarios
463 appear possible. ESCRT-III/Vps4 recruitment could be driven by ESCRT-0, -I or -II complexes
464 interacting with the ubiquitinated membrane proteins in these stalling endocytic buds. Indeed,
465 ESCRT-II mutants also genetically interact with *YPK1* (Fig. S1B). Alternatively, Bro1 – like
466 Alix in human cells - might help to recruit ESCRT-III directly to the PM. In budding yeast,
467 ESCRT-III subunits (Snf7) are also recruited to the PM during adaptation to alkaline pH and
468 are critically required for the regulator of Ime2 (RIM) pathway (80). Alternatively, changes in
469 PM tension might recruit the ESCRT machinery as described (81,82). Interestingly, ESCRT-
470 III subunits are recruited onto endosomal membranes when membrane tension is reduced (82).
471 In analogy, we speculate that ESCRT assemblies might recognize areas of decreased tension at
472 the PM.

473

474 Once there, the ESCRT machinery is involved in consolidating a slack PM. This might be
475 achieved either through stabilization of PM deformations, or via active remodeling (e.g.
476 removing (budding out) or deforming membranes), which could increase tension again. How
477 exactly ESCRT-III/Vps4 assemblies help to maintain the integrity of the PM in response to
478 tensile stress remains an open question at the moment.

479

480 The results from our genetic screen indicated that ESCRT-deficient cells are particularly
481 sensitive to perturbations in the homeostasis of two classes of lipids: the fungal cholesterol
482 analog ergosterol and sphingolipids. In concert, these lipids are known to promote membrane
483 rigidity and also to stabilize many membrane proteins (83-86). In yeast, they are important for
484 the formation of eisosomes (87), protein-coated membrane invaginations that have been
485 suggested to function as membrane reservoirs that can balance changes in membrane tension,
486 in analogy to caveolae (88-90). Moreover, eisosomes are involved in the regulation of TORC2
487 signaling (24). Sphingolipids and ergosterol might therefore become essential in ESCRT
488 mutants to counteract membrane stress.

489

490 Orm2 emerges here as a central player in membrane homeostasis. The accumulation of Orm2
491 at the ER in ESCRT mutants and/or in post-ER compartments in EGAD mutants causes
492 membrane stress in budding yeast, judged from increased activity of TORC2 (9). Hence
493 maintaining proper control of Orm2 levels is important to restrain SPT activity and prevent the
494 potentially toxic accumulation of metabolic intermediates, such as LCBs (91). Similarly, failure
495 to control ORMDL protein levels is associated with several disease conditions in humans
496 (15,18-21), which are probably connected to mis-regulation of SPT activity (92,93) and might
497 well involve increased susceptibility to membrane stress.

498

499 Levels of LCBs are usually tightly controlled on the levels of synthesis, degradation and
500 conversion into ceramides and complex SL (94,95). Primarily Ypk1 (and to a lesser extent
501 Ypk2) regulates flux of LCBs into complex SL through phosphorylation of the CS subunits
502 Lag1 and Lac1 (32). Failure to phosphorylate CS also causes accumulation of LCBs and
503 diminished formation of complex SL. Thus, we speculate that in *vps4*Δ *ypk1*Δ cells the
504 coordination of SPT and CS activity is lost. Probably SPT activity can still be to some degree
505 de-repressed by TORC2 via Ypk2, whereas CS activity cannot be efficiently stimulated when
506 Ypk1 is deleted (32). This may additionally be aggravated by the accumulation of Orm2 in the
507 ER, because high Orm2 levels can diverge Ypk1 (and hence probably also Ypk2) activity away
508 from other important targets (32). Collectively, this leads to a built up of LCBs in *vps4*Δ *ypk1*Δ
509 cells and the ensuing defects in membrane integrity. Consistently, mimicking phosphorylation
510 of Lag1 slightly improved the growth of *vps4*Δ *ypk1*Δ mutants (Fig. 3F).

511

512 The major culprit for the accumulation of Orm2 at the ER in ESCRT mutants appears to be its
513 premature dephosphorylation in a calcineurin-dependent manner, which decreases ER export
514 of Orm2 and thus slows down Orm2 degradation through the EGAD pathway. Calcineurin is
515 activated by elevated intracellular calcium levels, and calcineurin activity is probably increased
516 in ESCRT mutants (76). ESCRT mutants have been found to be sensitive to calcium, which
517 can be suppressed by calcineurin inhibition or by stimulating intracellular calcium storage
518 (75,96). *vps4*Δ mutants upregulate the Golgi calcium pump Pmr1 (97), possibly to decrease
519 intracellular calcium. Pmr1 is also essential for the survival of ESCRT mutants (9). Similarly,
520 Csg2 is required for growth under high calcium conditions (98) and for growth of *vps4*Δ
521 mutants (Fig. S1A), indicating tight links between the ESCRT machinery, calcium signaling
522 and the regulation of SL biosynthesis.
523
524 The growth defect of *vps4*Δ *ypk1*Δ double mutants was alleviated by calcineurin inhibition and
525 extracellular calcium chelation, suggesting that increased calcium uptake drives detrimental
526 calcineurin activity in these cells. Increased calcium influx in ESCRT mutants may be caused
527 by deregulated trafficking or turnover of the plasma membrane calcium channel (Cch1/Mid1),
528 which is likely a substrate of the ESCRT machinery. Mid1 could also respond to increased
529 membrane stress in ESCRT mutants, since Mid1 is a stretch-activated channel and allows
530 calcium influx and calcineurin signaling to respond to mechanical membrane stress (99).
531 Alternatively, ER-PM contact sites may be corrupted in ESCRT mutants. The disruption of
532 these contact sites leads to increased calcium influx and calcineurin activity, which increased
533 LCBs and decreased ceramide levels (60).
534
535 At the moment, it is unclear whether calcineurin directly dephosphorylates Orm2. The sequence
536 of Orm2 does not contain an obvious calcineurin binding site (100,101). The Cdc55-containing
537 protein phosphatase 2A (PP2A) controls Orm2 phosphorylation levels during heat shock (102).
538 Inactivation of Cdc55-PP2A or another phosphatase upon calcineurin-inhibition cannot be
539 ruled out as an indirect cause leading to dephosphorylation of Orm2, but to our knowledge has
540 not been reported. However, since calcineurin antagonizes TORC2 and Ypk1 activity also
541 towards other targets (29,32,74,103), it might also directly contribute to the phosphorylation
542 status of Orm2. In addition to lowering Orm2 protein levels, inhibition of calcineurin is also
543 expected to promote phosphorylation of the CS subunits Lag1/Lac1 and thereby formation of
544 ceramides, which mitigates the buildup of harmful LCBs (32). Thus, calcineurin inactivation

545 probably has several beneficial effects in ESCRT mutants, which collectively render their
546 growth largely independent of Ypk1 signaling.
547
548 In summary, we propose that ESCRT function maintains PM homeostasis on several levels: (i)
549 through the MVB pathway by degrading membrane proteins and preventing proteotoxic stress
550 (104), (ii) by preserving or repairing the PM in response to membrane stress, and (iii) by
551 maintaining calcium homeostasis, which is important for controlled output of TORC2-Ypk1
552 signaling and regulation of Orm2. The latter promotes biosynthetic SL flux and thereby
553 preserves PM homeostasis. In ESCRT mutants, regulation of Orm2 is disturbed because of
554 increased calcineurin-dependent dephosphorylation, and hence its ER export and turnover
555 through EGAD is impaired. The buildup of Orm2 protein levels in the ER constitutes a stress
556 that must be counteracted through increased TORC2-Ypk1 activity (Fig. S5D). As long as this
557 is possible, ESCRT mutants have little fitness defects. However, if phosphorylation of Orm2 is
558 additionally impaired by any means (deletion of *YPK1*; inhibition of TORC2), or if plasma
559 membrane homeostasis is acutely challenged, ESCRT mutants are no longer able to
560 compensate. Now their PM integrity becomes compromised, and viability decreases
561 dramatically. Importantly, the mutual dependence of the ESCRT machinery and TORC2-Ypk1
562 signaling was broken by reducing steady state levels of Orm2, either through deletion of the
563 gene, or by enforcing phosphorylation, ER export and degradation.
564
565 These findings demonstrate the importance of post-translational regulation of ORMDL family
566 proteins for membrane homeostasis, and establish ORMDL protein levels as a central
567 determinant of PM stress in eukaryotic cells. Our data connect the ESCRT machinery to PM
568 stress and deregulated calcineurin signaling, and explain how ESCRT mutants become addicted
569 to TORC2-dependent signaling.
570

571 **Experimental Procedures**

572

573 **Yeast strains, plasmids and growth conditions**

574 Genetic modifications were performed by PCR and/or homologous recombination using
575 standard techniques. Plasmid-expressed genes including their native promoters and terminators
576 were amplified from yeast genomic DNA and cloned into centromeric vectors (pRS series)
577 (105). Tagged version of Orm1 and Orm2 (3xHA, 3xFLAG, or GFP) and their respective
578 mutants were expressed from plasmids in the respective deletion mutants replacing the
579 endogenous protein (with exception of Fig. 5D, where *FLAG-Orm2* was co-expressed). All
580 constructs were analyzed by DNA-sequencing and transformed into yeast cells using standard
581 techniques. Genotypes of yeast strains and plasmids used in this study as well as primer for
582 PCR-based genetic modifications and cloning are listed in Table S2.

583

584 All *S. cerevisiae* strains in this study were SEY6210 derivatives. For liquid cultures, cells were
585 incubated in YNB synthetic medium supplemented with amino acids (according to respective
586 auxotrophies) and 2% glucose at 26°C in a shaker and were grown to midlog phase (OD_{600}=0.5
587 – 0.8). For growth on agar plates, yeast cells were diluted to OD_{600nm} = 0.05 and spotted in
588 serial dilutions on YPD or YNB (auxotrophic selection medium) plates at the indicated
589 conditions. Rapamycin (Sigma) was added at the indicated concentrations from a 1 mM stock
590 in DMSO and myriocin (Sigma) was added to 1.5 µM from a 5 mM stock in methanol.
591 Untreated controls were supplied with the appropriate amount of the respective solvent. For the
592 assessment of growth in presence of PalmC, cells were grown into log phase, diluted to an
593 OD_{600nm} of 0.1 into fresh YNB medium containing PalmC (Sigma) at the indicated
594 concentration (from a 5 mM stock in DMSO) and grown at 26°C, 180 rpm. For the assessment
595 of growth in presence of FK-506 (Sigma; stock 20 mg/ml in DMSO) or EGTA (Sigma; stock
596 500 mM in water) cells were grown into log phase, diluted to an OD_{600nm} of 0.05 into fresh
597 YPD medium containing 2 µg/ml FK-506 or 0.1 mM EGTA. After 24 hours the OD_{600nm} was
598 measured.

599

600 **Analysis of genetic interaction data**

601 Gene Ontology (GO) enrichment analysis (106) was performed using the 119 genes listed in
602 Appendix Table S1 of (9) as synthetically lethal with *vps4*Δ in two biological replicates or lethal
603 in one and sick in the other replicate. They were analyzed with the 'generic GO-Slim: process'
604 terms using the GO Slim mapper of the *Saccharomyces* genome database. GO term fusion and

605 enrichment analysis was performed as described (9). Only significantly scored GO terms ($p <$
606 0.05) are presented in Fig. 1A. The full analysis is presented in Table S1.
607
608 **Preparation of whole cell protein extracts, Western blot analysis and immunodetection**
609 To prepare whole cell lysates, proteins were extracted by alkaline extraction (107). When
610 protein phosphorylation was also analyzed, extraction was done by a modified protocol with
611 phosphatase inhibition as described (9). Protein extracts were denatured in Lämmli sample
612 buffer, separated by SDS-PAGE (Biorad Mini Protean) and transferred to PVDF membranes
613 by semi-dry electro-blotting. Phos-tag SDS PAGE as well as immunodetection of ubiquitinated
614 Orm2 were done as described (9). Antibodies used in this study are listed in Table S2.
615
616 **FLAG-Orm2 immunoprecipitations**
617 Immunoprecipitations of FLAG-Orm2 under denaturing or non-denaturing lysis conditions
618 were done as described in detail in (9).
619
620 **RNA isolation and quantitative PCR (RT-qPCR)**
621 RNA isolation, cDNA synthesis and quantitative RT-PCR analysis were performed as
622 described previously (9,108). TAQman gene expression assays were from Thermo Fisher
623 (*YPK1*: Sc04141261_s1; *ORM1*: Sc04125000_s1; *ORM2*: Sc04149509_s1; housekeeping gene
624 *PGK1*: Sc04104844_s1). RT-qPCR analysis was done from 4-6 independent biological samples
625 and each in 3-4 technical replicates. Data were analyzed with the PikoReal software (version
626 2.2; Thermo Scientific) with manual threshold adjustment, and relative mRNA abundance was
627 calculated in Microsoft Excel (Version 16.16.2; RRID:SCR_016137) using the $\Delta\Delta C_T$ method
628 (109).
629
630 **Fluorescence live cell wide field microscopy**
631 For microscopy, cells were grown to midlog (OD_{600}=0.5 – 0.8) phase in YNB media,
632 concentrated by centrifugation and directly mounted onto glass slides. For imaging of the Dsc
633 complex (Fig. S4B), cells were grown for 36 hours on selective YNB agar plates, dissolved in
634 sterile water and mounted for imaging. Live cell wide field fluorescence microscopy was
635 carried out using a Zeiss Axio Imager M1 equipped with a sola light engine LED light source
636 (Lumencore), a 100x oil immersion objective (NA 1.45,) standard GFP and mCherry
637 fluorescent filters, a SPOT Xplorer CCD camera, and Visitron VisiView software (version
638 2.1.4). The brightness and contrast of the images in the figures were adjusted using Photoshop

639 CS5 (Adobe Version 12.0.4x64; RRID:SCR_014199). For merged images the levels of red and
640 green channels were separately adjusted.
641
642 **Assessment of plasma membrane integrity by propidium iodide staining**
643 Cells were grown in YPD medium and kept in logarithmic growth phase for >12 hours. 1 ml of
644 culture was supplemented with 3 mg/ml propidium iodide (Sigma; stock 1 mg/ml in phosphate
645 buffered saline (PBS)) and incubated at RT for 10 minutes. Cells were recovered by
646 centrifugation (10000xg, 4°C, 2 min), washed once with 1 ml ice cold PBS, resuspended in 0.5
647 ml ice cold PBS and kept on ice. Propidium iodide-positive cells were counted on an Attune^{TM}
648 NxT Acoustic Focusing Cytometer (Life Technologies) with Attune^{TM} NxT software (v.
649 3.1.1243.0). Debris and cell doublets were excluded. Propidium iodide signal was measured
650 with 488 nm excitation and emission in the 695/40 nm window. In each experiment 50000 cells
651 of each genotype were counted. Gating was adjusted so that more than 99.9% of WT cells were
652 propidium iodide-negative.
653
654 **Immuno-gold electron microscopy**
655 As previously described (44) samples were high-pressure frozen, freeze-substituted and
656 rehydrated (110), followed by indirect immunogold labeling of 100 nm-thick, thawed
657 cryosections (44). Antibodies used were goat polyclonal anti GFP (1:500; Rockland) and rabbit
658 anti goat Fab' NANOGOLD™ (1:150; Nanoprobes). Transmission electron microscopy was
659 performed on a Philips CM120 (now: Thermo Fisher Scientific).
660
661 **Cycloheximide chase assay**
662 Logarithmically growing cells (20 OD_{600nm}) were harvested by centrifugation and cells were
663 resuspended in fresh medium to concentration of 0.4 OD/ml. 10 ml (4 OD_{600nm}) were
664 immediately (t = 0 min) harvested by centrifugation, washed once with ice-cold 10 mM NaF
665 solution, and pellets were snap frozen in liquid nitrogen. To the remaining culture 50 µg/ml
666 cycloheximide (Sigma Aldrich) was added from a 10 mg/ml stock. After the indicated time
667 points 10 ml culture were harvested, washed and frozen as above. Whole cell extracts were
668 prepared by alkaline extraction. SDS-PAGE, Western blot detection and quantification were
669 done as described (9).
670
671 **Metabolic sphingolipid labeling, sphingolipid extraction and thin layer chromatography**

672 Sphingolipid labeling and extraction were done as described previously (9,111).
673 Logarithmically growing cells (5 OD_{600nm}) were harvested by centrifugation and resuspended
674 in 470 µl fresh medium. 30 µCi of [^{3}H]-L-serine (1µCi/µl; Hartmann Analytic) was added and
675 cells were incubated at 30°C, 700 rpm for 5 hours. Proteins were precipitated with 4.5%
676 perchloric acid, cell pellets were washed with ice-cold 100mM EDTA, resuspended in 50µl
677 water, and subjected to mild alkaline methanolysis (50% methanol; 10% 1-butanol; 10%
678 monomethylamine; 50 minutes at 50°C) of ester lipids. Lysates were vacuum dried in a speed
679 vac (37°C), pellets were resuspended thoroughly in 300 µl water by sonication, and tritium-
680 incorporation of was assessed for normalization in duplicates by szintillation counting (LS6500,
681 Beckmann Coulter). Sphingolipids were extracted 3 times with water-saturated 1-butanol,
682 vacuum dried in a speed vac (37°C), and dissolved in 50 µl chloroform : methanol : water
683 10:10:3 for thin layer chromatography. Thin-layer chromatography (solvent system chloroform
684 : methanol : 4.2N ammonium hydroxide 9:7:2) was done as described (111) on aluminium silica
685 TLC plates (Sigma) for 75 minutes. Subsequently, plates were dried under air flow and treated
686 twice with En^{3}Hance autoradiography enhancer (Perkin-Elmer), dried again, and exposed to
687 autoradiography films (CL-Xposure Film, Thermo) at -80°C. The identity of labeled bands was
688 confirmed with specific mutant yeast strains or inhibitors (data not shown). A tritium-labeled
689 band X close to the solvent front that was observed previously (111) is not sensitive to myriocin
690 treatment (Sigma Aldrich, 1.5µM), suggesting that it is not a sphingolipid.
691
692 **Lipid extraction and liquid chromatography - mass spectrometry (LC-MS)**
693 For combined LCB and ceramide analysis (Fig. 3D) lipids were extracted from lysed yeast cells
694 according to 200 µg of protein by chloroform/methanol extraction (112). Prior to extraction an
695 internal standard mix containing sphingosine (LCB 17:0) and ceramide (CER 18:0/17:1) was
696 spiked into each sample for normalization. Quantification was done by external quantification
697 with the same lipids in different concentrations. Dried lipid samples were dissolved in a 65:35
698 mixture of mobile phase A (60:40 water/acetonitrile, including 10 mM ammonium formate and
699 0.1% formic acid) and mobile phase B (88:10:2 2-propanol/acetonitrile/H_20, including 2 mM
700 ammonium formate and 0.02% formic acid). HPLC analysis was performed employing a C30
701 reverse-phase column (Thermo Acclaim C30, 2.1 x 250 mm, 3 µm, operated at 40° C; Thermo
702 Fisher Scientific) connected to an HP 1100 series HPLC (Agilent) HPLC system and a
703 QExactive*PLUS* orbitrap mass spectrometer (Thermo Fisher Scientific) equipped with a heated
704 electrospray ionization (HESI) probe. The elution was performed with a gradient of 20 min;
705 from 0–1 min elution starts with 40% B and increases to 100% in a linear gradient over 13 min.

706 100% B is maintained for 3 mins. Afterwards solvent B was decreased to 40% and maintained
707 for another 3.8 minutes for column re-equilibration. The mass spectrometer was run in negative
708 and positive ion mode. The scan rate was set from 200-1200 m/z. Mass resolution was 70,000
709 with an AGC target of 3,000,000 and a maximum injection time of 100 ms. The MS was
710 operated in data dependent mode. For MS/MS the resolution was 35000 with a maximum
711 injection time of 50 ms and an AGC target of 100,000. The loop count was ten. Selected ions
712 were fragmented by HCD (higher energy collision dissociation) with a normalized collision
713 energy of 30. The dynamic exclusion list was set to 10s to avoid repetitive sequencing.
714 Ceramide peaks were identified using the Lipid Search algorithm (MKI, Tokyo, Japan). Peaks
715 were defined through raw files, product ion, and precursor ion accurate masses. Ceramides were
716 identified by database (>1,000,000 entries) search of negative ion adducts. LCBs were
717 identified by positive ion adducts. The accurate mass extracted ion chromatograms were
718 integrated for each identified lipid precursor and peak areas obtained for quantitation. Internal
719 standards were used for normalization and an external standard curve was used to calculate
720 absolute values (in pmol/µg protein). Ceramides are presented as the sum of all quantified
721 ceramide species. For comparison, data were normalized to WT levels (set to 1) of ceramide
722 and C18-PHS, respectively. Data are presented as mean ±standard deviation from three
723 independent experiments.
724
725 **Quantification and statistical analysis**
726 Statistical details and sample numbers of quantitative analyses can be found in the respective
727 figures and corresponding figure legends. Quantitative data is usually displayed as mean
728 ±standard deviation from at least 3 biological replicates and relates to the wildtype control.
729
730 **(i) GO analysis of genetic interaction data**
731 A hypergeometric test was used to estimate if the mapped GO term is significantly enriched
732 with the selected genes. The null hypothesis is that the selected genes are randomly sampled
733 from all yeast genes. The resulting p-values were corrected with the Benjamini-Hochberg
734 method. All adjusted p-values below 0.05 were reported.
735
736 **(ii) Quantification of Snf7-eGFP and Vps4-eGFP localization**
737 Images were taken in an unbiased manner by selecting and focusing cells only in brightfield
738 view. 50 cells of each genotype and condition were imaged and visually inspected for the

739 presence and number of eGFP puncta at the cell cortex. Cells were grouped into cohorts of 0-
740 2, 3-5 and more than 5 cortical eGFP puncta.
741
742 **(iii) Quantification of cell growth**
743 Cell growth after 2 hours in culture was measured photometrically by absorbance at 600 nm.
744 Measurements from 3 independent experiments (each with up to three parallel cultures
745 representing technical replicates) were presented with box-whisker plots indicating the median,
746 first and third quartile. Individual data points including outliers were also plotted.
747
748 **(iv) Quantification of Western Blot analysis**
749 Western blot signals were quantified by densitometry using ImageJ2 (Version 2.0.0-rc49/1.51h;
750 RRID:SCR_003070) (113), quantifications were exported to Microsoft Excel (Version 16.16.2;
751 RRID:SCR_016137), normalized to the respective Pgk1 loading controls, and presented as
752 mean ±standard deviation from at least three independent experiments. t=0 was set to 1.
753
754 **(v) Quantitative PCR (RT-qPCR)**
755 Mean, normalized $\Delta\Delta C_T$ values were individually calculated for four independent biological
756 replicates (each with 3-4 technical replicates), log2-transformed to calculate fold change, and
757 presented as mean fold change over WT ±standard deviation. A one-sided Student's t-test was
758 used on the mean $\Delta\Delta C_T$ values (i.e. prior to log transformation) of the four biological replicates
759 of to assess statistical significance.
760
761 **(vi) Lipid extraction and mass spectrometry**
762 Internal standards for ceramides (Cer 18:1;2/17:0;0) and LCBs (LCB 17:0) spiked in prior to
763 extraction were used for normalization and an external standard curve was used to calculate
764 absolute values (in pmol/µg protein). To compare data from different experimental setups, data
765 were normalized to WT levels of the most abundant LCB and ceramide species (C18-
766 phytosphingosine and Cer44:0;4). Data are presented as mean ±standard deviation from three
767 independent experiments.
768
769 **Data availability**
770
771 All relevant data has been included in the paper in main figures and supplemental information.
772

Acknowledgments

We would like to thank Theresa Dunn, Peter Espenshade, Ming Li and Howard Riezman for providing reagents, and Jennifer Kahlhofer and Manuel Haschka for help with flow cytometry.

Author contributions

O.S. performed the SL-TLC analyses and growth experiments; O.S., Y.W., S.S., M.A.W., V.B., R.L. and C.S. constructed yeast strains and plasmids and conducted microscopy, biochemical and genetic experiments; M.A. performed the statistical analysis of the GO dataset; M.H. performed electron microscopy; S.E. and F.F. analyzed ceramide and LCB levels; O.S., S.S. and D.T. analyzed data; O.S. and D.T. guided the story; O.S. and D.T. wrote the manuscript with input from all authors.

Funding and additional information

Work in the Teis laboratory was supported by the Austrian Science Fund (FWF-Y444-B12, P30263, P29583) and MCBO (W1101-B18) to D.T and EMBO/Marie Curie (ALTF 642-2012; EMBOCOFUND2010, GA-2010-267146), MUI-START (2013042023) and 'Tiroler Wissenschaftsfond' to O.S. The Stefan laboratory is supported by MRC funding to the MRC LMCB University Unit at UCL, award code MC_UU_00012/6.

Conflict of interest

The authors declare that they have no conflicts of interest with the contents of this article.

796 **References**

797 1. Ruggiano, A., Foresti, O., and Carvalho, P. (2014) Quality control: ER-associated
798 degradation: protein quality control and beyond. *J Cell Biol* **204**, 869-879
799 2. Wu, X., and Rapoport, T. A. (2018) Mechanistic insights into ER-associated protein
800 degradation. *Curr Opin Cell Biol* **53**, 22-28
801 3. Gil, G., Faust, J. R., Chin, D. J., Goldstein, J. L., and Brown, M. S. (1985) Membrane-
802 bound domain of HMG CoA reductase is required for sterol-enhanced degradation of
803 the enzyme. *Cell* **41**, 249-258
804 4. Hampton, R. Y., Gardner, R. G., and Rine, J. (1996) Role of 26S proteasome and
805 HRD genes in the degradation of 3-hydroxy-3-methylglutaryl-CoA reductase, an
806 integral endoplasmic reticulum membrane protein. *Mol Biol Cell* **7**, 2029-2044
807 5. Gill, S., Stevenson, J., Kristiana, I., and Brown, A. J. (2011) Cholesterol-dependent
808 degradation of squalene monooxygenase, a control point in cholesterol synthesis
809 beyond HMG-CoA reductase. *Cell Metab* **13**, 260-273
810 6. Foresti, O., Ruggiano, A., Hannibal-Bach, H. K., Ejsing, C. S., and Carvalho, P.
811 (2013) Sterol homeostasis requires regulated degradation of squalene monooxygenase
812 by the ubiquitin ligase Doa10/Teb4. *Elife* **2**, e00953
813 7. Strzyz, P. (2017) Unfolded protein response: Reacting to membrane stress. *Nat Rev*
814 *Mol Cell Biol* **18**, 471
815 8. Travers, K. J., Patil, C. K., Wodicka, L., Lockhart, D. J., Weissman, J. S., and Walter,
816 P. (2000) Functional and genomic analyses reveal an essential coordination between
817 the unfolded protein response and ER-associated degradation. *Cell* **101**, 249-258
818 9. Schmidt, O., Weyer, Y., Baumann, V., Widerin, M. A., Eising, S., Angelova, M.,
819 Schleiffer, A., Kremser, L., Lindner, H., Peter, M., Frohlich, F., and Teis, D. (2019)
820 Endosome and Golgi-associated degradation (EGAD) of membrane proteins regulates
821 sphingolipid metabolism. *EMBO J* **38**, e101433
822 10. Stewart, E. V., Nwosu, C. C., Tong, Z., Roguev, A., Cummins, T. D., Kim, D. U.,
823 Hayles, J., Park, H. O., Hoe, K. L., Powell, D. W., Krogan, N. J., and Espenshade, P.
824 J. (2011) Yeast SREBP cleavage activation requires the Golgi Dsc E3 ligase complex.
825 *Mol Cell* **42**, 160-171
826 11. Reggiori, F., and Pelham, H. R. (2001) Sorting of proteins into multivesicular bodies:
827 ubiquitin-dependent and -independent targeting. *Embo J* **20**, 5176-5186
828 12. Li, M., Koshi, T., and Emr, S. D. (2015) Membrane-anchored ubiquitin ligase
829 complex is required for the turnover of lysosomal membrane proteins. *J Cell Biol* **211**,
830 jcb.201505062-201505652
831 13. Dobzinski, N., Chuartzman, S. G., Kama, R., Schuldiner, M., and Gerst, J. E. (2015)
832 Starvation-Dependent Regulation of Golgi Quality Control Links the TOR Signaling
833 and Vacuolar Protein Sorting Pathways. *Cell Rep*
834 14. Tong, Z., Kim, M. S., Pandey, A., and Espenshade, P. J. (2014) Identification of
835 candidate substrates for the Golgi Tul1 E3 ligase using quantitative diGly proteomics
836 in yeast. *Mol Cell Proteomics* **13**, 2871-2882
837 15. Breslow, D. K., Collins, S. R., Bodenmiller, B., Aebersold, R., Simons, K.,
838 Shevchenko, A., Ejsing, C. S., and Weissman, J. S. (2010) Orm family proteins
839 mediate sphingolipid homeostasis. *Nature* **463**, 1048-1053
840 16. Han, G., Gupta, S. D., Gable, K., Bacikova, D., Sengupta, N., Somashekarappa, N.,
841 Proia, R. L., Harmon, J. M., and Dunn, T. M. (2019) The ORMs interact with
842 transmembrane domain 1 of Lcb1 and regulate serine palmitoyltransferase
843 oligomerization, activity and localization. *Biochim Biophys Acta Mol Cell Biol Lipids*
844 **1864**, 245-259
845 17. Clarke, B. A., Majumder, S., Zhu, H., Lee, Y. T., Kono, M., Li, C., Khanna, C., Blain,
846 H., Schwartz, R., Huso, V. L., Byrnes, C., Tuymetova, G., Dunn, T. M., Allende, M.

847 L., and Proia, R. L. (2019) The Ormdl genes regulate the sphingolipid synthesis
848 pathway to ensure proper myelination and neurologic function in mice. *Elife* **8**
849 18. Moffatt, M. F., Kabesch, M., Liang, L., Dixon, A. L., Strachan, D., Heath, S., Depner,
850 M., von Berg, A., Bufe, A., Rietschel, E., Heinzmann, A., Simma, B., Frischer, T.,
851 Willis-Owen, S. A., Wong, K. C., Illig, T., Vogelberg, C., Weiland, S. K., von Mutius,
852 E., Abecasis, G. R., Farrall, M., Gut, I. G., Lathrop, G. M., and Cookson, W. O.
853 (2007) Genetic variants regulating ORMDL3 expression contribute to the risk of
854 childhood asthma. *Nature* **448**, 470-473
855 19. Barrett, J. C., Hansoul, S., Nicolae, D. L., Cho, J. H., Duerr, R. H., Rioux, J. D., Brant,
856 S. R., Silverberg, M. S., Taylor, K. D., Barmada, M. M., Bitton, A., Dassopoulos, T.,
857 Datta, L. W., Green, T., Griffiths, A. M., Kistner, E. O., Murtha, M. T., Regueiro, M.
858 D., Rotter, J. I., Schumm, L. P., Steinhart, A. H., Targan, S. R., Xavier, R. J.,
859 Consortium, N. I. G., Libioulle, C., Sandor, C., Lathrop, M., Belaiche, J., Dewit, O.,
860 Gut, I., Heath, S., Laukens, D., Mni, M., Rutgeerts, P., Van Gossum, A., Zelenika, D.,
861 Franchimont, D., Hugot, J. P., de Vos, M., Vermeire, S., Louis, E., Belgian-French, I.
862 B. D. C., Wellcome Trust Case Control, C., Cardon, L. R., Anderson, C. A.,
863 Drummond, H., Nimmo, E., Ahmad, T., Prescott, N. J., Onnie, C. M., Fisher, S. A.,
864 Marchini, J., Ghori, J., Bumpstead, S., Gwilliam, R., Tremelling, M., Deloukas, P.,
865 Mansfield, J., Jewell, D., Satsangi, J., Mathew, C. G., Parkes, M., Georges, M., and
866 Daly, M. J. (2008) Genome-wide association defines more than 30 distinct
867 susceptibility loci for Crohn's disease. *Nat Genet* **40**, 955-962
868 20. McGovern, D. P., Gardet, A., Torkvist, L., Goyette, P., Essers, J., Taylor, K. D.,
869 Neale, B. M., Ong, R. T., Lagace, C., Li, C., Green, T., Stevens, C. R., Beauchamp,
870 C., Fleshner, P. R., Carlson, M., D'Amato, M., Halfvarson, J., Hibberd, M. L., Lordal,
871 M., Padyukov, L., Andriulli, A., Colombo, E., Latiano, A., Palmieri, O., Bernard, E.
872 J., Deslandres, C., Hommes, D. W., de Jong, D. J., Stokkers, P. C., Weersma, R. K.,
873 Consortium, N. I. G., Sharma, Y., Silverberg, M. S., Cho, J. H., Wu, J., Roeder, K.,
874 Brant, S. R., Schumm, L. P., Duerr, R. H., Dubinsky, M. C., Glazer, N. L.,
875 Haritunians, T., Ippoliti, A., Melmed, G. Y., Siscovick, D. S., Vasiliauskas, E. A.,
876 Targan, S. R., Annese, V., Wijmenga, C., Pettersson, S., Rotter, J. I., Xavier, R. J.,
877 Daly, M. J., Rioux, J. D., and Seielstad, M. (2010) Genome-wide association identifies
878 multiple ulcerative colitis susceptibility loci. *Nat Genet* **42**, 332-337
879 21. Barrett, J. C., Clayton, D. G., Concannon, P., Akolkar, B., Cooper, J. D., Erlich, H. A.,
880 Julier, C., Morahan, G., Nerup, J., Nierras, C., Plagnol, V., Pociot, F., Schuilenburg,
881 H., Smyth, D. J., Stevens, H., Todd, J. A., Walker, N. M., Rich, S. S., and Type 1
882 Diabetes Genetics, C. (2009) Genome-wide association study and meta-analysis find
883 that over 40 loci affect risk of type 1 diabetes. *Nat Genet* **41**, 703-707
884 22. Roelants, F. M., Breslow, D. K., Muir, A., Weissman, J. S., and Thorner, J. (2011)
885 Protein kinase Ypk1 phosphorylates regulatory proteins Orm1 and Orm2 to control
886 sphingolipid homeostasis in Saccharomyces cerevisiae. *Proc Natl Acad Sci U S A* **108**,
887 19222-19227
888 23. Kamada, Y., Fujioka, Y., Suzuki, N. N., Inagaki, F., Wullschleger, S., Loewith, R.,
889 Hall, M. N., and Ohsumi, Y. (2005) Tor2 directly phosphorylates the AGC kinase
890 Ypk2 to regulate actin polarization. *Mol Cell Biol* **25**, 7239-7248
891 24. Berchtold, D., Piccolis, M., Chiaruttini, N., Riezman, I., Riezman, H., Roux, A.,
892 Walther, T. C., and Loewith, R. (2012) Plasma membrane stress induces relocalization
893 of Slm proteins and activation of TORC2 to promote sphingolipid synthesis. *Nat Cell*
894 *Biol* **14**, 542-547
895 25. Riggi, M., Niewola-Staszkowska, K., Chiaruttini, N., Colom, A., Kusmider, B.,
896 Mercier, V., Soleimanpour, S., Stahl, M., Matile, S., Roux, A., and Loewith, R. (2018)

897 Decrease in plasma membrane tension triggers PtdIns(4,5)P2 phase separation to
898 inactivate TORC2. *Nat Cell Biol* **20**, 1043-1051
899 26. Aronova, S., Wedaman, K., Aronov, P. A., Fontes, K., Ramos, K., Hammock, B. D.,
900 and Powers, T. (2008) Regulation of ceramide biosynthesis by TOR complex 2. *Cell*
901 *Metab* **7**, 148-158
902 27. Berchtold, D., and Walther, T. C. (2009) TORC2 plasma membrane localization is
903 essential for cell viability and restricted to a distinct domain. *Mol Biol Cell* **20**, 1565-
904 1575
905 28. Locke, M. N., and Thorner, J. (2019) Rab5 GTPases are required for optimal TORC2
906 function. *J Cell Biol* **218**, 961-976
907 29. Niles, B. J., Mogri, H., Hill, A., Vlahakis, A., and Powers, T. (2012) Plasma
908 membrane recruitment and activation of the AGC kinase Ypk1 is mediated by target
909 of rapamycin complex 2 (TORC2) and its effector proteins Slm1 and Slm2. *Proc Natl*
910 *Acad Sci U S A* **109**, 1536-1541
911 30. Liao, H. C., and Chen, M. Y. (2012) Target of rapamycin complex 2 signals to
912 downstream effector yeast protein kinase 2 (Ypk2) through adheres-voraciously-to-
913 target-of-rapamycin-2 protein 1 (Avo1) in Saccharomyces cerevisiae. *J Biol Chem*
914 **287**, 6089-6099
915 31. Rispal, D., Eltschinger, S., Stahl, M., Vaga, S., Bodenmiller, B., Abraham, Y.,
916 Filipuzzi, I., Movva, N. R., Aebersold, R., Helliwell, S. B., and Loewith, R. (2015)
917 Target of Rapamycin Complex 2 Regulates Actin Polarization and Endocytosis via
918 Multiple Pathways. *J Biol Chem* **290**, 14963-14978
919 32. Muir, A., Ramachandran, S., Roelants, F. M., Timmons, G., and Thorner, J. (2014)
920 TORC2-dependent protein kinase Ypk1 phosphorylates ceramide synthase to
921 stimulate synthesis of complex sphingolipids. *Elife* **3**
922 33. Roelants, F. M., Baltz, A. G., Trott, A. E., Fereres, S., and Thorner, J. (2010) A
923 protein kinase network regulates the function of aminophospholipid flippases. *Proc*
924 *Natl Acad Sci U S A* **107**, 34-39
925 34. Lee, Y. J., Jeschke, G. R., Roelants, F. M., Thorner, J., and Turk, B. E. (2012)
926 Reciprocal phosphorylation of yeast glycerol-3-phosphate dehydrogenases in
927 adaptation to distinct types of stress. *Mol Cell Biol* **32**, 4705-4717
928 35. Muir, A., Roelants, F. M., Timmons, G., Leskoske, K. L., and Thorner, J. (2015)
929 Down-regulation of TORC2-Ypk1 signaling promotes MAPK-independent survival
930 under hyperosmotic stress. *Elife* **4**
931 36. Roelants, F. M., Leskoske, K. L., Pedersen, R. T. A., Muir, A., Liu, J. M., Finnigan,
932 G. C., and Thorner, J. (2017) TOR Complex 2-Regulated Protein Kinase Fpk1
933 Stimulates Endocytosis via Inhibition of Ark1/Prk1-Related Protein Kinase Akl1 in
934 Saccharomyces cerevisiae. *Mol Cell Biol* **37**
935 37. Hatakeyama, R., Kono, K., and Yoshida, S. (2017) Ypk1 and Ypk2 kinases maintain
936 Rho1 at the plasma membrane by flippase-dependent lipid remodeling after membrane
937 stresses. *J Cell Sci* **130**, 1169-1178
938 38. Alvaro, C. G., Aindow, A., and Thorner, J. (2016) Differential Phosphorylation
939 Provides a Switch to Control How alpha-Arrestin Rod1 Down-regulates Mating
940 Pheromone Response in Saccharomyces cerevisiae. *Genetics* **203**, 299-317
941 39. Chen, P., Lee, K. S., and Levin, D. E. (1993) A pair of putative protein kinase genes
942 (YPK1 and YPK2) is required for cell growth in Saccharomyces cerevisiae. *Mol Gen*
943 *Genet* **236**, 443-447
944 40. Schöneberg, J., Lee, I.-H., Iwasa, J. H., and Hurley, J. H. (2017) Reverse-topology
945 membrane scission by the ESCRT proteins. *Nature reviews Molecular cell biology* **18**,
946 5-17

947 41. Vietri, M., Radulovic, M., and Stenmark, H. (2019) The many functions of ESCRTs.
948 *Nat Rev Mol Cell Biol*
949 42. Migliano, S. M., and Teis, D. (2018) ESCRT and Membrane Protein Ubiquitination.
950 *Prog Mol Subcell Biol* **57**, 107-135
951 43. Odorizzi, G., Babst, M., and Emr, S. D. (1998) Fab1p PtdIns(3)P 5-kinase function
952 essential for protein sorting in the multivesicular body. *Cell* **95**, 847-858
953 44. Adell, M. A. Y., Migliano, S. M., Upadhyayula, S., Bykov, Y. S., Sprenger, S.,
954 Pakdel, M., Vogel, G. F., Jih, G., Skillern, W., Behrouzi, R., Babst, M., Schmidt, O.,
955 Hess, M. W., Briggs, J. A., Kirchhausen, T., and Teis, D. (2017) Recruitment
956 dynamics of ESCRT-III and Vps4 to endosomes and implications for reverse
957 membrane budding. *Elife* **6**
958 45. Zhu, L., Jorgensen, J. R., Li, M., Chuang, Y. S., and Emr, S. D. (2017) ESCRTs
959 function directly on the lysosome membrane to downregulate ubiquitinated lysosomal
960 membrane proteins. *Elife* **6**
961 46. Yang, X., Zhang, W., Wen, X., Bulinski, P. J., Chomchai, D. A., Arines, F. M., Liu,
962 Y. Y., Sprenger, S., Teis, D., Klionsky, D. J., and Li, M. (2020) TORC1 regulates
963 vacuole membrane composition through ubiquitin- and ESCRT-dependent
964 microautophagy. *J Cell Biol* **219**
965 47. Hatakeyama, R., Peli-Gulli, M. P., Hu, Z., Jaquenoud, M., Garcia Osuna, G. M.,
966 Sardu, A., Dengjel, J., and De Virgilio, C. (2019) Spatially Distinct Pools of TORC1
967 Balance Protein Homeostasis. *Mol Cell* **73**, 325-338 e328
968 48. Raymond, C. K., Howald-Stevenson, I., Vater, C. A., and Stevens, T. H. (1992)
969 Morphological classification of the yeast vacuolar protein sorting mutants: evidence
970 for a prevacuolar compartment in class E vps mutants. *Mol Biol Cell* **3**, 1389-1402
971 49. Gatta, A. T., and Carlton, J. G. (2019) The ESCRT-machinery: closing holes and
972 expanding roles. *Curr Opin Cell Biol* **59**, 121-132
973 50. Radulovic, M., Schink, K. O., Wenzel, E. M., Nahse, V., Bongiovanni, A., Lafont, F.,
974 and Stenmark, H. (2018) ESCRT-mediated lysosome repair precedes lysophagy and
975 promotes cell survival. *EMBO J* **37**
976 51. Vietri, M., Schink, K. O., Campsteijn, C., Wegner, C. S., Schultz, S. W., Christ, L.,
977 Thoresen, S. B., Brech, A., Raiborg, C., and Stenmark, H. (2015) Spastin and ESCRT-
978 III coordinate mitotic spindle disassembly and nuclear envelope sealing. *Nature* **522**,
979 231-235
980 52. Olmos, Y., Hodgson, L., Mantell, J., Verkade, P., and Carlton, J. G. (2015) ESCRT-III
981 controls nuclear envelope reformation. *Nature* **522**, 236-239
982 53. Webster, B. M., Colombi, P., Jager, J., and Lusk, C. P. (2014) Surveillance of nuclear
983 pore complex assembly by ESCRT-III/Vps4. *Cell* **159**, 388-401
984 54. Skowyra, M. L., Schlesinger, P. H., Naismith, T. V., and Hanson, P. I. (2018)
985 Triggered recruitment of ESCRT machinery promotes endolysosomal repair. *Science*
986 **360**
987 55. McCullough, J., Clippinger, A. K., Talledge, N., Skowyra, M. L., Saunders, M. G.,
988 Naismith, T. V., Colf, L. A., Afonine, P., Arthur, C., Sundquist, W. I., Hanson, P. I.,
989 and Frost, A. (2015) Structure and membrane remodeling activity of ESCRT-III
990 helical polymers. *Science*
991 56. Jimenez, A. J., Maiuri, P., Lafaurie-Janvore, J., Divoux, S., Piel, M., and Perez, F.
992 (2014) ESCRT machinery is required for plasma membrane repair. *Science* **343**,
993 1247136
994 57. Raab, M., Gentili, M., de Belly, H., Thiam, H. R., Vargas, P., Jimenez, A. J.,
995 Lautenschlaeger, F., Voituriez, R., Lennon-Dumenil, A. M., Manel, N., and Piel, M.
996 (2016) ESCRT III repairs nuclear envelope ruptures during cell migration to limit
997 DNA damage and cell death. *Science* **352**, 359-362

998 58. Denais, C. M., Gilbert, R. M., Isermann, P., McGregor, A. L., te Lindert, M.,
999 Weigelin, B., Davidson, P. M., Friedl, P., Wolf, K., and Lammerding, J. (2016)
1000 Nuclear envelope rupture and repair during cancer cell migration. *Science* **352**, 353-
1001 358
1002 59. Roelants, F. M., Leskoske, K. L., Martinez Marshall, M. N., Locke, M. N., and
1003 Thorner, J. (2017) The TORC2-Dependent Signaling Network in the Yeast
1004 Saccharomyces cerevisiae. *Biomolecules* **7**
1005 60. Omnus, D. J., Manford, A. G., Bader, J. M., Emr, S. D., and Stefan, C. J. (2016)
1006 Phosphoinositide kinase signaling controls ER-PM cross-talk. *Mol Biol Cell* **27**, 1170-
1007 1180
1008 61. Bauer, I., Brune, T., Preiss, R., and Köllinger, R. (2015) Evidence for a Non-
1009 endosomal Function of the Saccharomyces cerevisiae ESCRT-III Like Protein Chm7.
1010 *Genetics* **115.178939**
1011 62. Roelants, F. M., Torrance, P. D., Bezman, N., and Thorner, J. (2002) Pkh1 and Pkh2
1012 differentially phosphorylate and activate Ypk1 and Ykr2 and define protein kinase
1013 modules required for maintenance of cell wall integrity. *Mol Biol Cell* **13**, 3005-3028
1014 63. deHart, A. K., Schnell, J. D., Allen, D. A., and Hicke, L. (2002) The conserved Pkh-
1015 Ypk kinase cascade is required for endocytosis in yeast. *J Cell Biol* **156**, 241-248
1016 64. Gaubitz, C., Oliveira, T. M., Prouteau, M., Leitner, A., Karuppasamy, M.,
1017 Konstantinidou, G., Rispal, D., Eltschinger, S., Robinson, G. C., Thore, S., Aebersold,
1018 R., Schaffitzel, C., and Loewith, R. (2015) Molecular Basis of the Rapamycin
1019 Insensitivity of Target Of Rapamycin Complex 2. *Mol Cell* **58**, 977-988
1020 65. Riggi, M., Bourgoint, C., Macchione, M., Matile, S., Loewith, R., and Roux, A.
1021 (2019) TORC2 controls endocytosis through plasma membrane tension. *J Cell Biol*
1022 **218**, 2265-2276
1023 66. Ruhl, S., Shkarina, K., Demarco, B., Heilig, R., Santos, J. C., and Broz, P. (2018)
1024 ESCRT-dependent membrane repair negatively regulates pyroptosis downstream of
1025 GSDMD activation. *Science* **362**, 956-960
1026 67. Gong, Y. N., Guy, C., Olauson, H., Becker, J. U., Yang, M., Fitzgerald, P.,
1027 Linkermann, A., and Green, D. R. (2017) ESCRT-III Acts Downstream of MLKL to
1028 Regulate Necroptotic Cell Death and Its Consequences. *Cell* **169**, 286-300 e216
1029 68. Scheffer, L. L., Sreetama, S. C., Sharma, N., Medikayala, S., Brown, K. J., Defour, A.,
1030 and Jaiswal, J. K. (2014) Mechanism of Ca(2)(+)-triggered ESCRT assembly and
1031 regulation of cell membrane repair. *Nat Commun* **5**, 5646
1032 69. Leskoske, K. L., Roelants, F. M., Martinez Marshall, M. N., Hill, J. M., and Thorner,
1033 J. (2017) The Stress-Sensing TORC2 Complex Activates Yeast AGC-Family Protein
1034 Kinase Ypk1 at Multiple Novel Sites. *Genetics* **207**, 179-195
1035 70. Shimobayashi, M., Takematsu, H., Eiho, K., Yamane, Y., and Kozutsumi, Y. (2010)
1036 Identification of Ypk1 as a novel selective substrate for nitrogen starvation-triggered
1037 proteolysis requiring autophagy system and endosomal sorting complex required for
1038 transport (ESCRT) machinery components. *J Biol Chem* **285**, 36984-36994
1039 71. Guillas, I., Kirchman, P. A., Chuard, R., Pfefferli, M., Jiang, J. C., Jazwinski, S. M.,
1040 and Conzelmann, A. (2001) C26-CoA-dependent ceramide synthesis of
1041 Saccharomyces cerevisiae is operated by Lag1p and Lac1p. *EMBO J* **20**, 2655-2665
1042 72. Schorling, S., Vallee, B., Barz, W. P., Riezman, H., and Oesterhelt, D. (2001) Lag1p
1043 and Lac1p are essential for the Acyl-CoA-dependent ceramide synthase reaction in
1044 Saccharomyces cerevisae. *Mol Biol Cell* **12**, 3417-3427
1045 73. Yang, X., Arines, F. M., Zhang, W., and Li, M. (2018) Sorting of a multi-subunit
1046 ubiquitin ligase complex in the endolysosome system. *Elife* **7**
1047 74. Mulet, J. M., Martin, D. E., Loewith, R., and Hall, M. N. (2006) Mutual antagonism of
1048 target of rapamycin and calcineurin signaling. *J Biol Chem* **281**, 33000-33007

1049 75. Zhao, Y., Du, J., Zhao, G., and Jiang, L. (2013) Activation of calcineurin is mainly
1050 responsible for the calcium sensitivity of gene deletion mutations in the genome of
1051 budding yeast. *Genomics* **101**, 49-56
1052 76. Zhao, Y., Du, J., Xiong, B., Xu, H., and Jiang, L. (2013) ESCRT components regulate
1053 the expression of the ER/Golgi calcium pump gene PMR1 through the Rim101/Nrg1
1054 pathway in budding yeast. *J Mol Cell Biol* **5**, 336-344
1055 77. Cyert, M. S., and Thorner, J. (1992) Regulatory subunit (CNB1 gene product) of yeast
1056 Ca2+/calmodulin-dependent phosphoprotein phosphatases is required for adaptation to
1057 pheromone. *Mol Cell Biol* **12**, 3460-3469
1058 78. Gururaj, C., Federman, R. S., and Chang, A. (2013) Orm proteins integrate multiple
1059 signals to maintain sphingolipid homeostasis. *J Biol Chem* **288**, 20453-20463
1060 79. Yoshimoto, H., Saltsman, K., Gasch, A. P., Li, H. X., Ogawa, N., Botstein, D., Brown,
1061 P. O., and Cyert, M. S. (2002) Genome-wide analysis of gene expression regulated by
1062 the calcineurin/Crz1p signaling pathway in Saccharomyces cerevisiae. *J Biol Chem*
1063 **277**, 31079-31088
1064 80. Obara, K., and Kihara, A. (2014) Signaling events of the Rim101 pathway occur at the
1065 plasma membrane in a ubiquitination-dependent manner. *Mol Cell Biol* **34**, 3525-3534
1066 81. Lafaurie-Janvore, J., Maiuri, P., Wang, I., Pinot, M., Manneville, J. B., Betz, T.,
1067 Balland, M., and Piel, M. (2013) ESCRT-III assembly and cytokinetic abscission are
1068 induced by tension release in the intercellular bridge. *Science* **339**, 1625-1629
1069 82. [preprint] Mercier, V., Larios, J., Molinard, G., Goujon, A., Matile, S., Gruenberg, J.,
1070 and Roux, A. (2019) ENDOSOMAL MEMBRANE TENSION CONTROLS ESCRT-
1071 III-DEPENDENT INTRA-LUMENAL VESICLE FORMATION. *bioRxiv*, 550483
1072 83. Bieberich, E. (2018) Sphingolipids and lipid rafts: Novel concepts and methods of
1073 analysis. *Chem Phys Lipids* **216**, 114-131
1074 84. Guan, X. L., Souza, C. M., Pichler, H., Dewhurst, G., Schaad, O., Kajiwara, K.,
1075 Wakabayashi, H., Ivanova, T., Castillon, G. A., Piccolis, M., Abe, F., Loewith, R.,
1076 Funato, K., Wenk, M. R., and Riezman, H. (2009) Functional interactions between
1077 sphingolipids and sterols in biological membranes regulating cell physiology. *Mol*
1078 *Biol Cell* **20**, 2083-2095
1079 85. Castro, B. M., Silva, L. C., Fedorov, A., de Almeida, R. F., and Prieto, M. (2009)
1080 Cholesterol-rich fluid membranes solubilize ceramide domains: implications for the
1081 structure and dynamics of mammalian intracellular and plasma membranes. *J Biol*
1082 *Chem* **284**, 22978-22987
1083 86. Megyeri, M., Riezman, H., Schuldiner, M., and Futerman, A. H. (2016) Making Sense
1084 of the Yeast Sphingolipid Pathway. *J Mol Biol* **428**, 4765-4775
1085 87. Walther, T. C., Brickner, J. H., Aguilar, P. S., Bernales, S., Pantoja, C., and Walter, P.
1086 (2006) Eisosomes mark static sites of endocytosis. *Nature* **439**, 998-1003
1087 88. Moseley, J. B. (2018) Eisosomes. *Curr Biol* **28**, R376-R378
1088 89. Athanasopoulos, A., Andre, B., Sophianopoulou, V., and Gournas, C. (2019) Fungal
1089 plasma membrane domains. *FEMS Microbiol Rev*
1090 90. Appadurai, D., Gay, L., Moharir, A., Lang, M. J., Duncan, M. C., Schmidt, O., Teis,
1091 D., Vu, T. N., Silva, M., Jorgensen, E. M., and Babst, M. (2019) Plasma membrane
1092 tension regulates eisosome structure and function. *Mol Biol Cell*, mbcE19040218
1093 91. Johnson, S. S., Hanson, P. K., Manoharlal, R., Brice, S. E., Cowart, L. A., and Moye-
1094 Rowley, W. S. (2010) Regulation of yeast nutrient permease endocytosis by ATP-
1095 binding cassette transporters and a seven-transmembrane protein, RSB1. *J Biol Chem*
1096 **285**, 35792-35802
1097 92. Worgall, T. S., Veerappan, A., Sung, B., Kim, B. I., Weiner, E., Bholah, R., Silver, R.
1098 B., Jiang, X. C., and Worgall, S. (2013) Impaired sphingolipid synthesis in the
1099 respiratory tract induces airway hyperreactivity. *Sci Transl Med* **5**, 186ra167

1100 93. Davis, D., Kannan, M., and Wattenberg, B. (2018) Orm/ORMDL proteins: Gate
1101 guardians and master regulators. *Adv Biol Regul* **70**, 3-18
1102 94. Frohlich, F., Petit, C., Kory, N., Christiano, R., Hannibal-Bach, H. K., Graham, M.,
1103 Liu, X., Ejsing, C. S., Farese, R. V., and Walther, T. C. (2015) The GARP complex is
1104 required for cellular sphingolipid homeostasis. *Elife* **4**
1105 95. Olson, D. K., Frohlich, F., Farese, R. V., Jr., and Walther, T. C. (2016) Taming the
1106 sphinx: Mechanisms of cellular sphingolipid homeostasis. *Biochim Biophys Acta*
1107 **1861**, 784-792
1108 96. Zhao, Y., Xiong, B., Xu, H., and Jiang, L. (2014) Expression of NYV1 encoding the
1109 negative regulator of Pmc1 is repressed by two transcriptional repressors, Nrg1 and
1110 Mig1. *FEBS Lett* **588**, 3195-3201
1111 97. Müller, M., Schmidt, O., Angelova, M., Faserl, K., Weys, S., Kremser, L.,
1112 Pfaffenwimmer, T., Dalik, T., Kraft, C., Trajanoski, Z., Lindner, H., Teis, D., and
1113 Mizushima, N. (2015) The coordinated action of the MVB pathway and autophagy
1114 ensures cell survival during starvation. *Elife* **4**, e07736
1115 98. Beeler, T., Gable, K., Zhao, C., and Dunn, T. (1994) A novel protein, CSG2p, is
1116 required for Ca2+ regulation in Saccharomyces cerevisiae. *J Biol Chem* **269**, 7279-
1117 7284
1118 99. Mishra, R., van Drogen, F., Dechant, R., Oh, S., Jeon, N. L., Lee, S. S., and Peter, M.
1119 (2017) Protein kinase C and calcineurin cooperatively mediate cell survival under
1120 compressive mechanical stress. *Proc Natl Acad Sci U S A* **114**, 13471-13476
1121 100. Goldman, A., Roy, J., Bodenmiller, B., Wanka, S., Landry, C. R., Aebersold, R., and
1122 Cyert, M. S. (2014) The calcineurin signaling network evolves via conserved kinase-
1123 phosphatase modules that transcend substrate identity. *Mol Cell* **55**, 422-435
1124 101. Rodriguez, A., Roy, J., Martinez-Martinez, S., Lopez-Maderuelo, M. D., Nino-
1125 Moreno, P., Orti, L., Pantoja-Uceda, D., Pineda-Lucena, A., Cyert, M. S., and
1126 Redondo, J. M. (2009) A conserved docking surface on calcineurin mediates
1127 interaction with substrates and immunosuppressants. *Mol Cell* **33**, 616-626
1128 102. Sun, Y., Miao, Y., Yamane, Y., Zhang, C., Shokat, K. M., Takematsu, H., Kozutsumi,
1129 Y., and Drubin, D. G. (2012) Orm protein phosphoregulation mediates transient
1130 sphingolipid biosynthesis response to heat stress via the Pkh-Ypk and Cdc55-PP2A
1131 pathways. *Mol Biol Cell* **23**, 2388-2398
1132 103. Vlahakis, A., Graef, M., Nunnari, J., and Powers, T. (2014) TOR complex 2-Ypk1
1133 signaling is an essential positive regulator of the general amino acid control response
1134 and autophagy. *Proc Natl Acad Sci U S A* **111**, 10586-10591
1135 104. Zhao, Y., Macgurn, J. A., Liu, M., and Emr, S. (2013) The ART-Rsp5 ubiquitin ligase
1136 network comprises a plasma membrane quality control system that protects yeast cells
1137 from proteotoxic stress. *Elife* **2**, e00459
1138 105. Sikorski, R. S., and Hieter, P. (1989) A system of shuttle vectors and yeast host strains
1139 designed for efficient manipulation of DNA in Saccharomyces cerevisiae. *Genetics*
1140 **122**, 19-27
1141 106. Harris, M. A., Clark, J., Ireland, A., Lomax, J., Ashburner, M., Foulger, R., Eilbeck,
1142 K., Lewis, S., Marshall, B., Mungall, C., Richter, J., Rubin, G. M., Blake, J. A., Bult,
1143 C., Dolan, M., Drabkin, H., Eppig, J. T., Hill, D. P., Ni, L., Ringwald, M.,
1144 Balakrishnan, R., Cherry, J. M., Christie, K. R., Costanzo, M. C., Dwight, S. S.,
1145 Engel, S., Fisk, D. G., Hirschman, J. E., Hong, E. L., Nash, R. S., Sethuraman, A.,
1146 Theesfeld, C. L., Botstein, D., Dolinski, K., Feierbach, B., Berardini, T., Mundodi, S.,
1147 Rhee, S. Y., Apweiler, R., Barrell, D., Camon, E., Dimmer, E., Lee, V., Chisholm, R.,
1148 Gaudet, P., Kibbe, W., Kishore, R., Schwarz, E. M., Sternberg, P., Gwinn, M.,
1149 Hannick, L., Wortman, J., Berriman, M., Wood, V., de la Cruz, N., Tonellato, P.,

1150 Jaiswal, P., Seigfried, T., and White, R. (2004) The Gene Ontology (GO) database and
1151 informatics resource. *Nucleic Acids Res* **32**, D258-261
1152 107. Kushnirov, V. V. (2000) Rapid and reliable protein extraction from yeast. *Yeast* **16**,
1153 857-860
1154 108. Schmidt, O., Weyer, Y., Fink, M. J., Muller, M., Weys, S., Bindreither, M., and Teis,
1155 D. (2017) Regulation of Rab5 isoforms by transcriptional and post-transcriptional
1156 mechanisms in yeast. *FEBS Lett* **591**, 2803-2815
1157 109. Livak, K. J., and Schmittgen, T. D. (2001) Analysis of relative gene expression data
1158 using real-time quantitative PCR and the 2(-Delta Delta C(T)) Method. *Methods* **25**,
1159 402-408
1160 110. van Donselaar, E., Posthuma, G., Zeuschner, D., Humbel, B. M., and Slot, J. W.
1161 (2007) Immunogold labeling of cryosections from high-pressure frozen cells. *Traffic*
1162 **8**, 471-485
1163 111. Tabuchi, M., Audhya, A., Parsons, A. B., Boone, C., and Emr, S. D. (2006) The
1164 phosphatidylinositol 4,5-biphosphate and TORC2 binding proteins Slm1 and Slm2
1165 function in sphingolipid regulation. *Mol Cell Biol* **26**, 5861-5875
1166 112. Ejsing, C. S., Sampaio, J. L., Surendranath, V., Duchoslav, E., Ekroos, K., Klemm, R.
1167 W., Simons, K., and Shevchenko, A. (2009) Global analysis of the yeast lipidome by
1168 quantitative shotgun mass spectrometry. *Proc Natl Acad Sci U S A* **106**, 2136-2141
1169 113. Rueden, C. T., Schindelin, J., Hiner, M. C., DeZonia, B. E., Walter, A. E., Arena, E.
1170 T., and Eliceiri, K. W. (2017) ImageJ2: ImageJ for the next generation of scientific
1171 image data. *BMC Bioinformatics* **18**, 529
1172
1173

1174 **Abbreviations and nomenclature**

1175 AAA – ATPase associated with diverse cellular activities

1176 CS – ceramide synthase

1177 DHS – dihydrosphingosine

1178 Dsc – defective in SPRBP cleavage

1179 EGAD – endosome and Golgi-associated degradation

1180 EGTA – Ethylene glycol-bis(2-aminoethylether)-N,N,N′,N′-tetraacetic acid

1181 ER – endoplasmic reticulum

1182 ERAD – endoplasmic reticulum-associated degradation

1183 ESCRT – endosomal sorting complex(es) required for transport

1184 GO – gene ontology

1185 HMGR – 3-hydroxy-3-methylglutaryl coenzyme A reductase

1186 IP – immunoprecipitation

1187 IPC – inositolphosphoryl ceramide

1188 LCB – long chanin base

1189 LC-MS – liquid chromatography – mass spectrometry

1190 MVB – multivesicular body

1191 Orm2-3A – Orm2 serine 46,47,48 to alanine mutant (non-phosphorylatable)

1192 Orm2-3D – Orm2 serine 46,47,48 to aspartic acid mutant (phospho-mimetic)

1193 ORMDL – Orosomucoid-like protein (mammalian Orm1/2 paralogues)

1194 SGK1 – serum and glucocorticoid-induced kinase 1

1195 PalmC – palmitoyl carnitine

1196 PHS – phytosphingosine

1197 PI – propidium iodide

1198 PM – plasma membrane

1199 RIM – regulator of Ime2

1200 SL - sphingolipid

1201 SPOTS – SPT-Orm1/2-Tsc3-Sac1 complex

1202 SPT – serine-palmitoyl-coenzyme A transferase

1203 SREBP – sterol-responsive element binding protein

1204 TORC1/2 – target of rapamycin complex 1/2

1205 UPR – unfolded protein response

1206 WT – wildtype

1207

1208

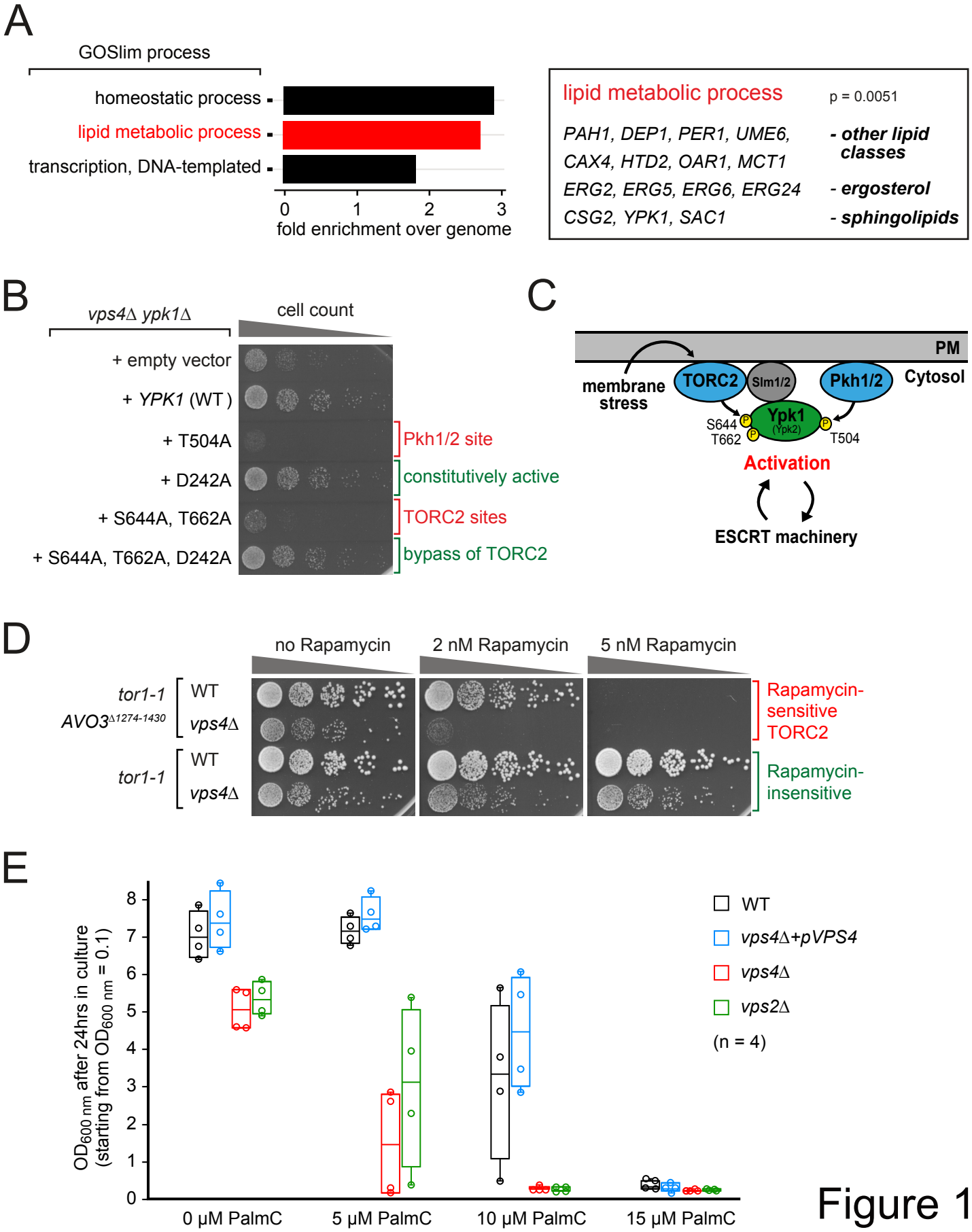
A
GOSlim process
homeostatic process
lipid metabolic process
transcription, DNA-templated
0
1
2
3
fold enrichment over genome
lipid metabolic process
p = 0.0051
PAH1, DEP1, PER1, UME6, CAX4, HTD2, OAR1, MCT1
- other lipid classes
ERG2, ERG5, ERG6, ERG24
- ergosterol
CSG2, YPK1, SAC1
- sphingolipids
B
vps4Δ ypk1Δ
cell count
+ empty vector
+ YPK1 (WT)
+ T504A
+ D242A
+ S644A, T662A
+ S644A, T662A, D242A
Pkh1/2 site
constitutively active
TORC2 sites
bypass of TORC2
C
PM
membrane stress
TORC2
Slm1/2
Pkh1/2
Cytosol
Ypk1
(Ypk2)
S644
T662
T504
Activation
ESCRT machinery
D
no Rapamycin
2 nM Rapamycin
5 nM Rapamycin
tor1-1
AVO3Δ1274-1430
WT
vps4Δ
tor1-1
WT
vps4Δ
Rapamycin-sensitive TORC2
Rapamycin-insensitive
E
OD600 nm after 24hrs in culture (starting from OD600 nm = 0.1)
0
1
2
3
4
5
6
7
8
0 μM PalmC
5 μM PalmC
10 μM PalmC
15 μM PalmC
WT
vps4Δ+pVPS4
vps4Δ
vps2Δ
(n = 4)

Figure 1

Figure 1: ESCRT mutants depend on lipid metabolism and TORC2-Ypk1 signaling for growth.

(A) Gene Ontology (GO) analysis for cellular processes of 119 genes that showed negative genetic interactions with *vps4*Δ (9). Only significantly enriched GO terms ($p < 0.05$) are shown. 15 genes comprised in the GO term 'lipid metabolic process' are shown. Full GO analysis in Table S1.

(B) Equal amounts of *vps4*Δ *ypk1*Δ double mutants expressing the indicated *YPK1* mutant plasmids (or empty vector) in serial dilutions were incubated on auxotrophic selection medium agar plates at 26°C.

(C) Schematic representation of the activation of the TORC2-Ypk1 signaling pathway in response to membrane stress and its putative interdependence with the ESCRT machinery. PM, plasma membrane; TORC2, target of rapamycin complex 2; Pkh1/2, yeast orthologues of 3-phosphoinositide-dependent kinase 1.

(D) Equal amounts of the indicated strains in serial dilutions were incubated on auxotrophic auxotrophic selection medium agar plates containing the indicated rapamycin concentrations at 26°C. All WT strains are the respective *vps4*Δ strain re-expressing *VPS4* from plasmid.

(E) Growth of the indicated strains in presence of palmitoyl-carnitine (PalmC). Cells were inoculated to $OD_{600nm} = 0.1$ in auxotrophic selection medium containing the indicated PalmC concentrations and grown for 24 hours in 4 independent experiments. The circles indicate the individual measurements.

See also Figure S1 and Table S1.

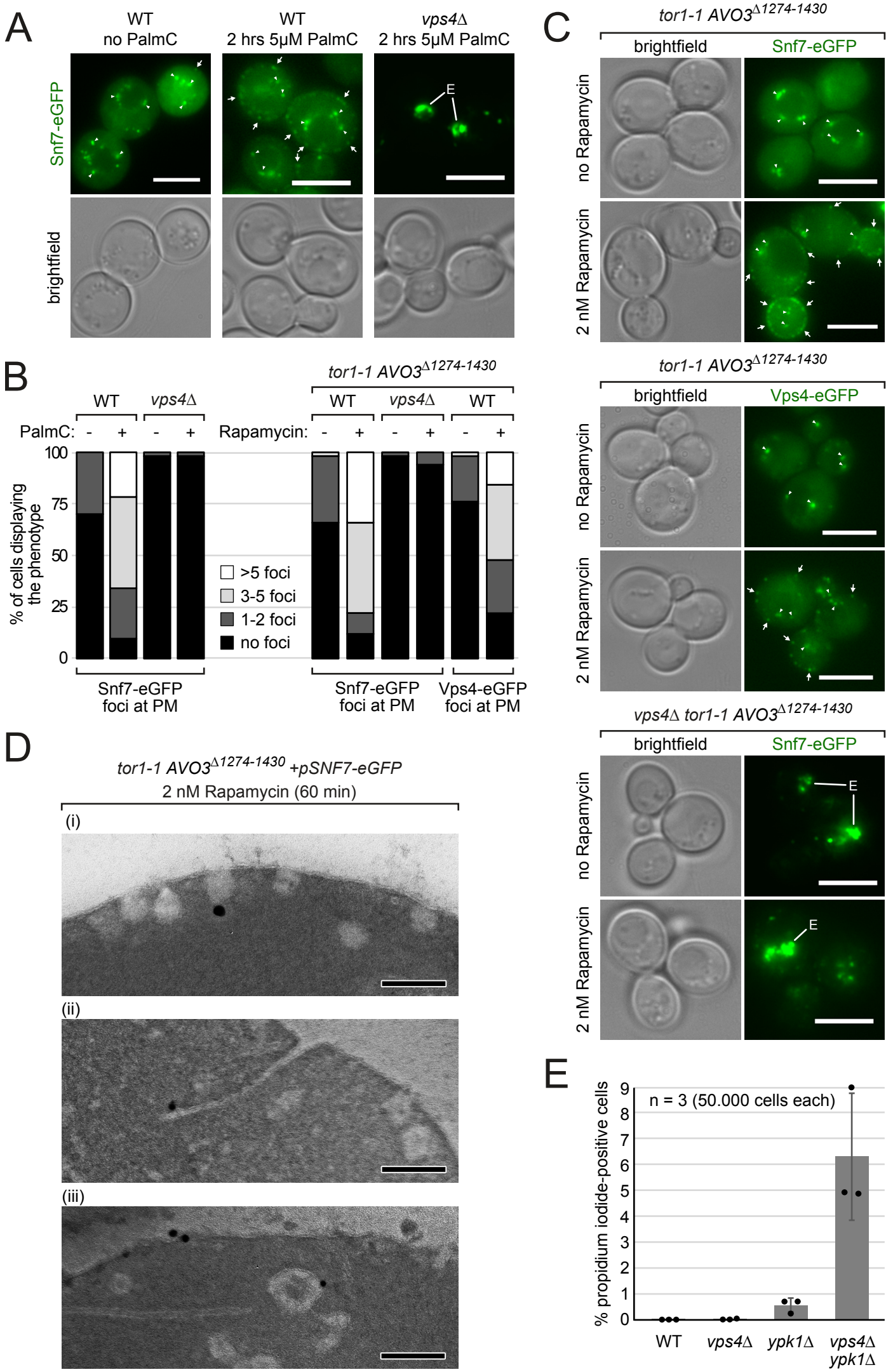
A
WT
no PalmC
WT
2 hrs 5μM PalmC
vps4Δ
2 hrs 5μM PalmC
Snf7-eGFP
brightfield
E
B
tor1-1 AVO3Δ1274-1430
WT
vps4Δ
WT
vps4Δ
WT
PalmC: - + - +
Rapamycin: - + - + - + - +
% of cells displaying the phenotype
100
75
50
25
0
>5 foci
3-5 foci
1-2 foci
no foci
Snf7-eGFP foci at PM
Snf7-eGFP foci at PM
Vps4-eGFP foci at PM
C
tor1-1 AVO3Δ1274-1430
brightfield
Snf7-eGFP
no Rapamycin
2 nM Rapamycin
tor1-1 AVO3Δ1274-1430
brightfield
Vps4-eGFP
no Rapamycin
2 nM Rapamycin
vps4Δ tor1-1 AVO3Δ1274-1430
brightfield
Snf7-eGFP
no Rapamycin
2 nM Rapamycin
E
D
tor1-1 AVO3Δ1274-1430 +pSNF7-eGFP
2 nM Rapamycin (60 min)
(i)
(ii)
(iii)
E
% propidium iodide-positive cells
n = 3 (50.000 cells each)
9
8
7
6
5
4
3
2
1
0
WT
vps4Δ
ypk1Δ
vps4Δ ypk1Δ

Figure 2

Figure 2: ESCRT-III/Vps4 assemblies form at the plasma membrane.

(A)-(D) All WT strains are isogenic to the respective *vps4*Δ cells and re-express *VPS4* (or *VPS4-eGFP* where indicated) from a plasmid.

(A) Epifluorescence and phase contrast microscopy of WT and *vps4*Δ cells co-expressing Snf7-eGFP (green) from a centromeric plasmid and treated with 5 µM palmitoyl-carnitine (PalmC) or vehicle (DMSO) for 2 hours. Arrowheads indicate Snf7 on endosomes/MVBs and arrows indicate Snf7 assemblies at the PM. Scale bars 5µm.

(B) Quantification of (B) and (C). Sub-cortical eGFP dots in 50 cells of each genotype and condition were counted and grouped into the indicated cohorts.

(C) Epifluorescence and phase contrast microscopy of the indicated strains co-expressing *SNF7-eGFP* or expressing *VPS4-eGFP* from centromeric plasmids and treated with 2nM rapamycin or vehicle (DMSO) for 2 hours. Arrowheads indicate endosomes/MVBs and arrows indicate Snf7/Vps4 assemblies at the PM. Scale bars 5µm.

(D) High-pressure freezing, anti-GFP immunogold labeling and transmission electron microscopy of the indicated cells treated with 2nM rapamycin for 60 minutes. Scale bars 200 nm.

(E) The indicated strains were grown into mid-log phase and stained with propidium iodide for 10 minutes. 50.000 cells were analyzed by flow cytometry. Data are presented as mean ±standard deviation from 3 independent experiments.

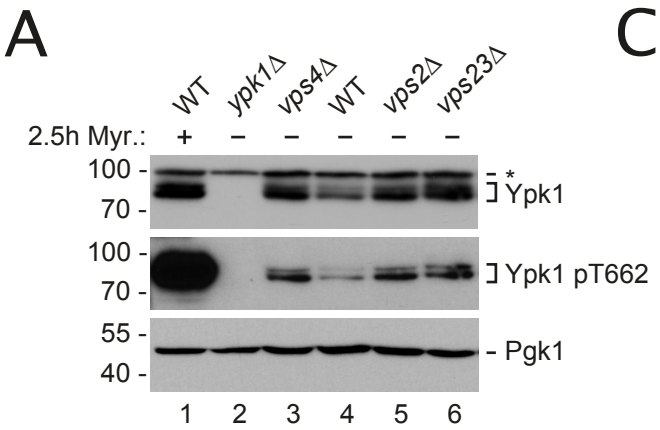
A
WT
ypk1Δ
vps4Δ
WT
vps2Δ
vps23Δ
2.5h Myr.: + – – – – –
100
70
Ypk1
100
70
Ypk1 pT662
55
40
Pgk1
1 2 3 4 5 6

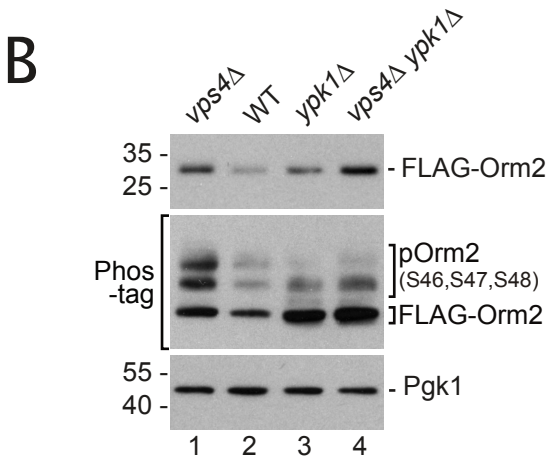
B
vps4Δ
WT
ypk1Δ
vps4Δ ypk1Δ
35
25
FLAG-Orm2
Phos
-tag
pOrm2
(S46,S47,S48)
FLAG-Orm2
55
40
Pgk1
1 2 3 4

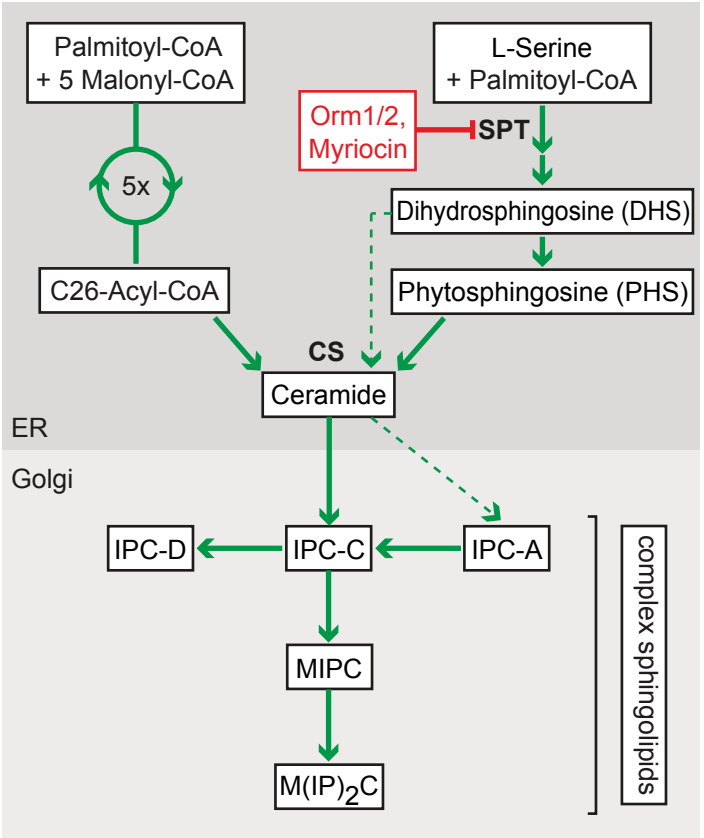
C
Palmitoyl-CoA
+ 5 Malonyl-CoA
L-Serine
+ Palmitoyl-CoA
Orm1/2,
Myriocin
SPT
5x
Dihydrosphingosine (DHS)
C26-Acyl-CoA
Phytosphingosine (PHS)
CS
Ceramide
ER
Golgi
IPC-D
IPC-C
IPC-A
complex sphingolipids
MIPC
M(IP)2C

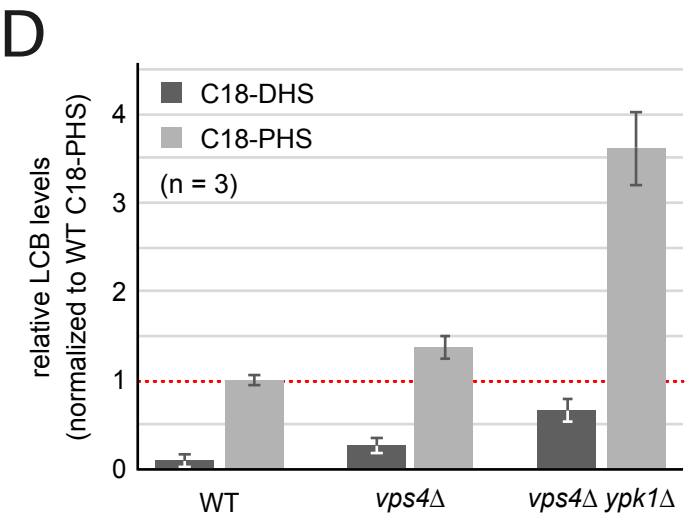
D
C18-DHS
C18-PHS
(n = 3)
relative LCB levels
(normalized to WT C18-PHS)
0
1
2
3
4
WT
vps4Δ
vps4Δ ypk1Δ

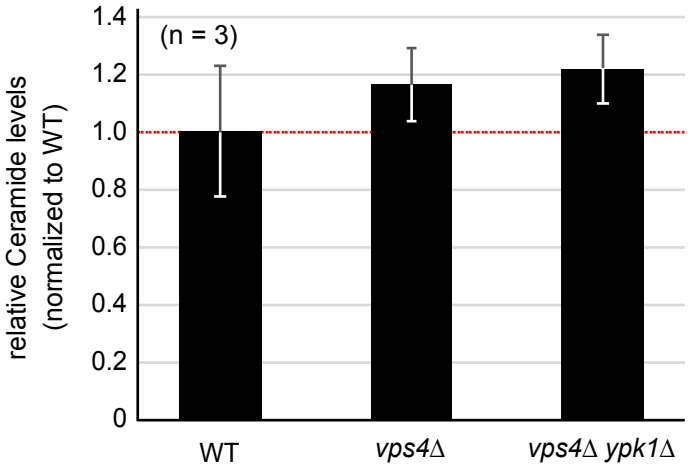
(n = 3)
relative Ceramide levels
(normalized to WT)
0
0.2
0.4
0.6
0.8
1.0
1.2
1.4
WT
vps4Δ
vps4Δ ypk1Δ

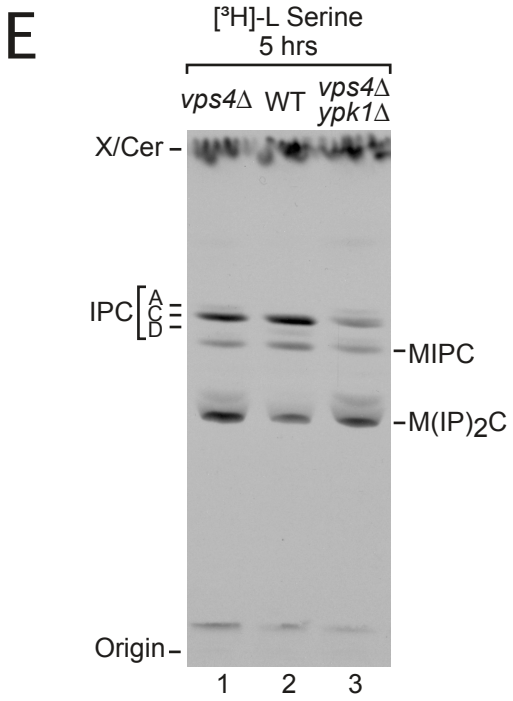
E
[³H]-L Serine
5 hrs
vps4Δ
WT
vps4Δ
ypk1Δ
X/Cer
IPC
A
C
D
MIPC
M(IP)2C
Origin
1 2 3

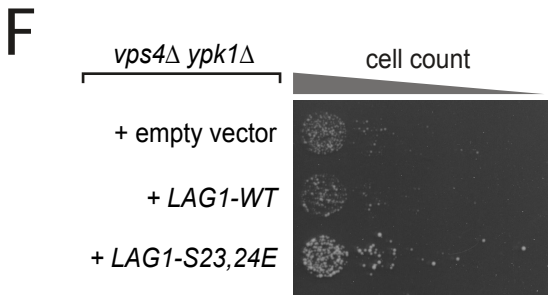
F
vps4Δ ypk1Δ
cell count
+ empty vector
+ LAG1-WT
+ LAG1-S23,24E

Figure 3

Figure 3: TORC2-Ypk1 signaling maintains sphingolipid homeostasis and prevents accumulation of long chain bases in ESCRT mutant cells.

(A) SDS-PAGE and Western blot analysis with the indicated antibodies of total yeast lysates from WT cells and the indicated mutants. Myr., myriocin (1.5µM; 2.5 h)

(B) SDS-PAGE or Phos-tag SDS PAGE and Western blot analysis with the indicated antibodies of total yeast lysates from WT cells and the indicated mutants expressing *FLAG-ORM2* (in *orm2*Δ background).

(C) Schematic representation of SL biosynthesis in *S. cerevisiae*. SPT, serine-palmitoyl-coenzyme A transferase; CS, ceramide synthase; IPC, Inositolphosphorylceramide; MIPC, mannosylinositolphosphorylceramide; MIP_2C, mannosyldiinositolphosphorylceramide.

(D) The levels of the long-chain bases (LCB) C18-dihydrosphingosine (C18-DHS) and C18-phytosphingosine (C18-PHS) and of ceramides (presented as the sum of all species) in lipid extracts from WT cells, *vps4Δ* and *vps4*Δ *ypk1*Δ mutants were measured using LC-MS and quantified using non-yeast LCBs/ceramides as external standards. Data are normalized to WT levels of C18-PHS and ceramide (set to 1) and presented as mean ± standard deviation from 3 independent experiments.

(E) Autoradiogram of sphingolipid extracts from [^{3}H]-serine radiolabeled WT cells and the indicated mutants that were separated by thin layer chromatography. X indicates an unknown lipid species that is insensitive to myriocin treatment (data not shown).

(F) Equal amounts of *vps4*Δ *ypk1*Δ cells expressing the indicated plasmids were spotted in serial dilutions on a YPD agar plate and incubated at 26°C.

See also Figure S3.

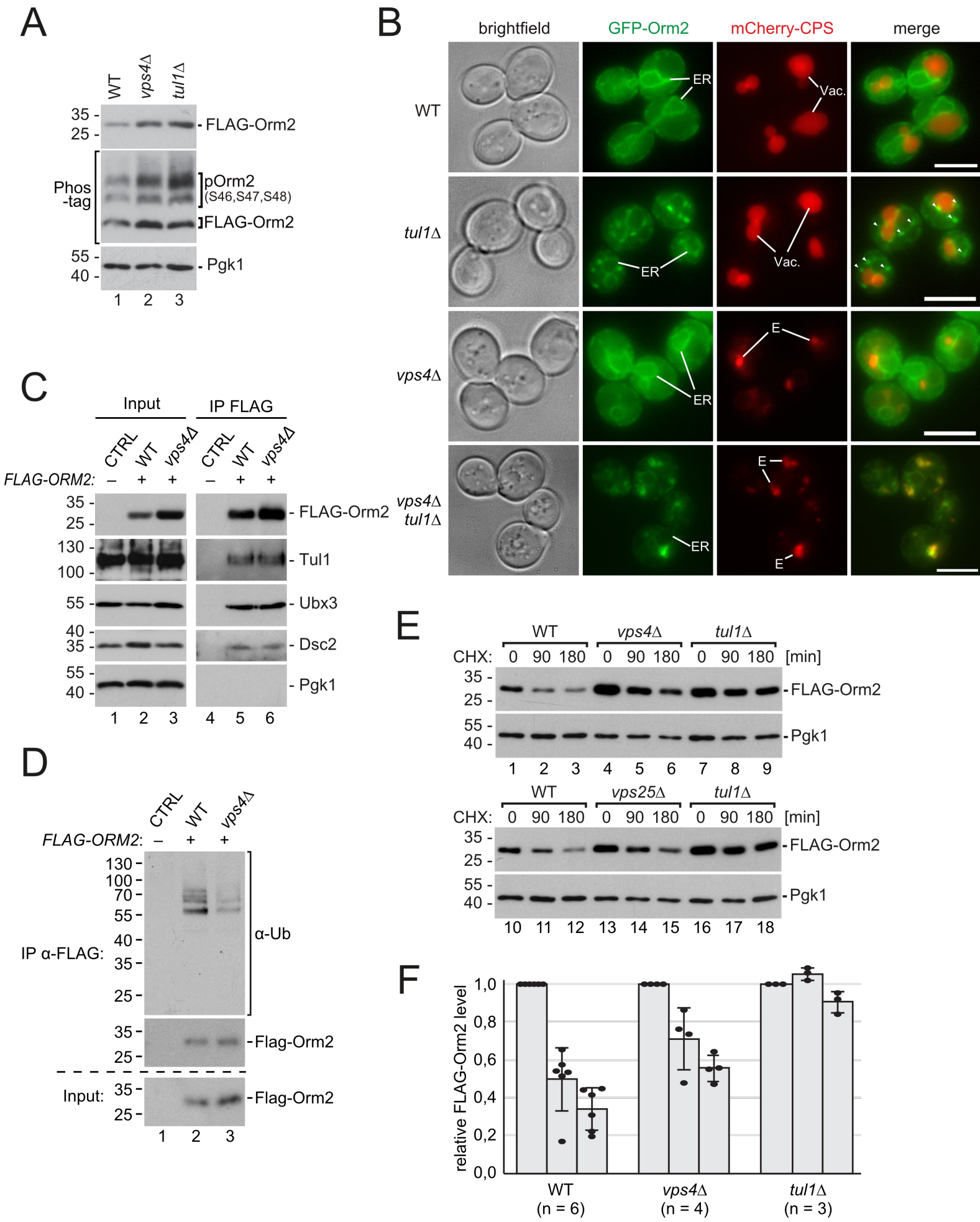
A
WT
vps4Δ
tul1Δ
35
25
FLAG-Orm2
Phos
-tag
pOrm2
(S46,S47,S48)
FLAG-Orm2
55
40
Pgk1
1 2 3
B
brightfield
GFP-Orm2
mCherry-CPS
merge
WT
tul1Δ
vps4Δ
vps4Δ
tul1Δ
ER
Vac.
E
C
Input
IP FLAG
CTRL
WT
vps4Δ
FLAG-ORM2:
FLAG-Orm2
130
100
Tul1
Ubx3
Dsc2
Pgk1
1 2 3 4 5 6
D
CTRL
WT
vps4Δ
FLAG-ORM2:
130
100
70
55
40
35
25
IP α-FLAG:
α-Ub
Flag-Orm2
Input:
Flag-Orm2
1 2 3
E
WT
vps4Δ
tul1Δ
CHX:
0 90 180 0 90 180 0 90 180 [min]
FLAG-Orm2
Pgk1
1 2 3 4 5 6 7 8 9
vps25Δ
10 11 12 13 14 15 16 17 18
F
relative FLAG-Orm2 level
1,0
0,8
0,6
0,4
0,2
0,0
WT
(n = 6)
vps4Δ
(n = 4)
tul1Δ
(n = 3)

Figure 4

Figure 4: ER export of Orm2 is impaired in ESCRT mutants.

(A) SDS-PAGE and Phos-tag SDS PAGE and Western blot analysis with the indicated antibodies of total yeast lysates from WT cells and the indicated mutants expressing *FLAG-ORM2*.

(B) Epifluorescence and phase contrast microscopy of living WT cells and the indicated mutants expressing GFP-Orm2 WT (green) and mCherry-CPS (red). ER, endoplasmic reticulum; Vac, vacuole; E, class E compartment. Arrowheads indicate GFP-Orm2 accumulations in post-ER compartments. Scale bars 5µm.

(C) SDS-PAGE and Western blot analysis with the indicated antibodies of input and elution (with FLAG peptide) from native FLAG-Orm2 immunoprecipitations (IP) from WT cells and *vps4*Δ mutants. Control cells expressed untagged Orm2.

(D) SDS-PAGE and Western blot analysis with the indicated antibodies of input and elution (with FLAG peptide) from denaturing FLAG-Orm2 immunoprecipitations from WT cells and *vps4*Δ mutants.

(E) WT cells and the indicated mutants were left untreated (0 min) or were treated with cycloheximide (CHX) to block protein synthesis for 90 min and 180 min at 26°C. Total cell lysates were analyzed by SDS-PAGE and Western blotting with the indicated antibodies.

(F) Graphs display the FLAG-Orm2 protein levels determined by densitometric quantification of Western blots from cell lysates of WT cells and the indicated mutants 0, 90 and 180 min after the addition of CHX. Each experiment was repeated at least three times, FLAG-Orm2 levels were normalized to Pgk1 loading controls, and each time-point was related to t=0 min (set to 1). Data are presented as mean ±standard deviation.

(A-F) All strains are in *orm2*Δ background.

See also Figure S4.

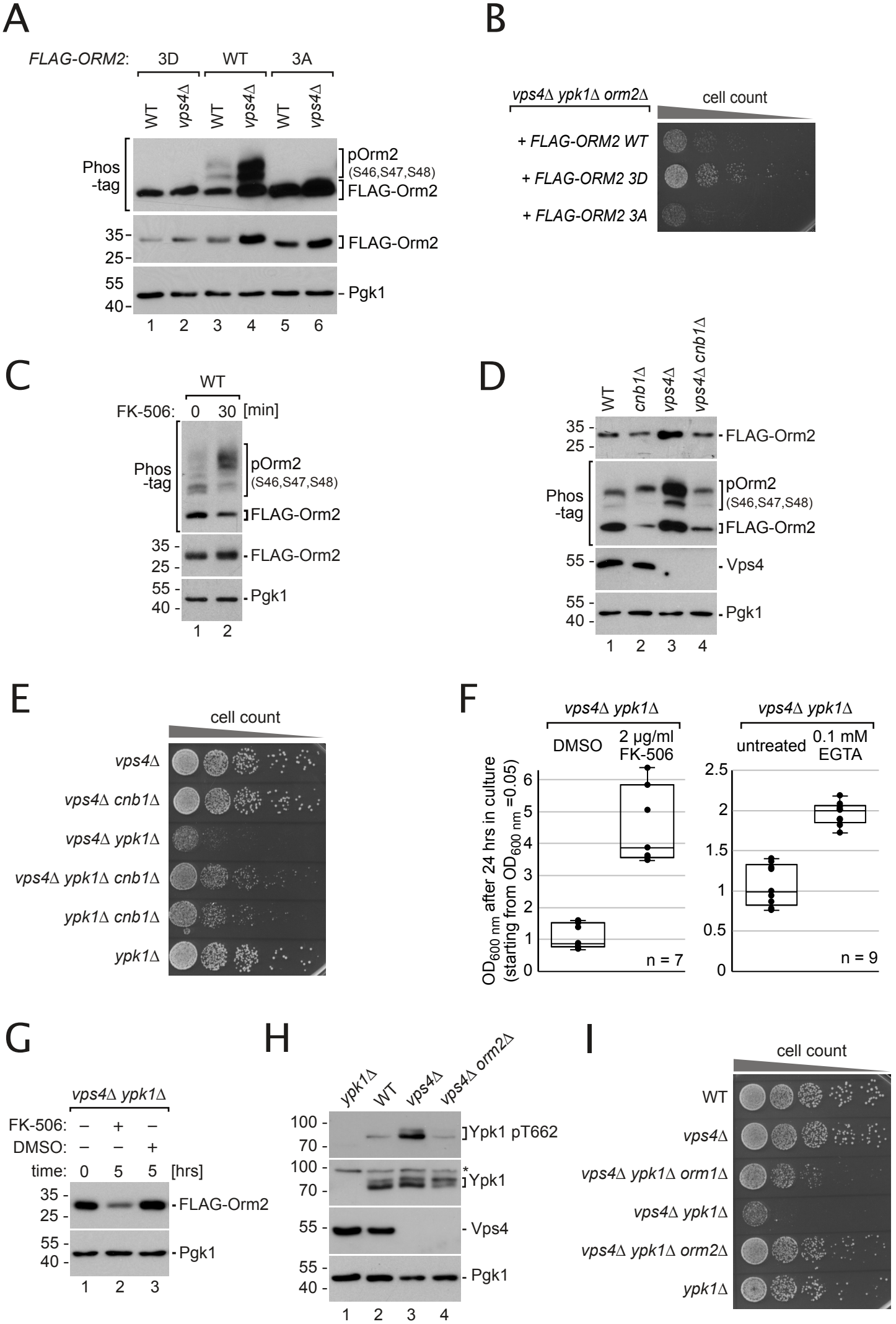
A
FLAG-ORM2: 3D WT 3A
WT vps4Δ WT vps4Δ WT vps4Δ
Phos -tag
pOrm2 (S46,S47,S48)
FLAG-Orm2
35 25
FLAG-Orm2
55 40
Pgk1
1 2 3 4 5 6
B
vps4Δ ypk1Δ orm2Δ
cell count
+ FLAG-ORM2 WT
+ FLAG-ORM2 3D
+ FLAG-ORM2 3A
C
WT
FK-506: 0 30 [min]
Phos -tag
pOrm2 (S46,S47,S48)
FLAG-Orm2
35 25
FLAG-Orm2
55 40
Pgk1
1 2
D
WT cnb1Δ vps4Δ vps4Δ cnb1Δ
35 25
FLAG-Orm2
Phos -tag
pOrm2 (S46,S47,S48)
FLAG-Orm2
55
Vps4
55 40
Pgk1
1 2 3 4
E
cell count
vps4Δ
vps4Δ cnb1Δ
vps4Δ ypk1Δ
vps4Δ ypk1Δ cnb1Δ
ypk1Δ cnb1Δ
ypk1Δ
F
vps4Δ ypk1Δ
DMSO
2 µg/ml FK-506
OD600 nm after 24 hrs in culture (starting from OD600 nm =0.05)
n = 7
vps4Δ ypk1Δ
untreated
0.1 mM EGTA
n = 9
G
vps4Δ ypk1Δ
FK-506: – + –
DMSO: – – +
time: 0 5 5 [hrs]
35 25
FLAG-Orm2
55 40
Pgk1
1 2 3
H
ypk1Δ WT vps4Δ vps4Δ orm2Δ
100 70
Ypk1 pT662
100 70
*
Ypk1
55
Vps4
55 40
Pgk1
1 2 3 4
I
cell count
WT
vps4Δ
vps4Δ ypk1Δ orm1Δ
vps4Δ ypk1Δ
vps4Δ ypk1Δ orm2Δ
ypk1Δ

Figure 5

Figure 5: Orm2 accumulation causes membrane stress in ESCRT mutants

(A) SDS-PAGE or Phos-tag SDS PAGE and Western blot analysis with the indicated antibodies of total yeast lysates from WT or *vps4*Δ cells expressing *FLAG-ORM2-WT, -3A or -3D* (in *orm2*Δ background).

(B) Equal amounts of *vps4*Δ *ypk1*Δ *orm2*Δ cells expressing the indicated *FLAG-ORM2* plasmids were spotted in serial dilutions on a auxotrophic selection medium agar plate and incubated at 26°C.

(C) SDS-PAGE and Phos-tag SDS PAGE and Western blot analysis with the indicated antibodies of total yeast lysates from WT cells expressing *FLAG-ORM2* (in *orm2*Δ background) treated with FK-506 (2 µg/ml) for the indicated time.

(D) SDS-PAGE and Phos-tag SDS PAGE and Western blot analysis with the indicated antibodies of total yeast lysates from WT cells and the indicated mutants expressing *FLAG-ORM2*.

(E) Equal amounts of the indicated single, double or triple mutants in serial dilutions were incubated on a YPD agar plate at 26°C.

(F) Left: Growth of *vps4*Δ *ypk1*Δ cells in YPD medium in presence of 2 µg/ml FK-506 or vehicle (DMSO). Right: Growth of *vps4*Δ *ypk1*Δ cells in YPD medium in presence of 0.1 mM EGTA or untreated. Cells were inoculated to OD_{600nm} = 0.05 and grown for 24 hours in 3 independent experiments. The circles indicate the individual measurements (7 and 9 technical replicates).

(G) SDS-PAGE PAGE and Western blot analysis with the indicated antibodies of total yeast lysates from *vps4*Δ *ypk1*Δ cells expressing *FLAG-ORM2* (in *orm2*Δ background) treated with FK-506 (2 µg/ml) or vehicle (DMSO) for the indicated time.

(H) SDS-PAGE and Western blot analysis with the indicated antibodies of total yeast lysates from WT cells and the indicated mutants.

(I) Equal amounts of WT cells and indicated single, double or triple mutants in serial dilutions were incubated on a YPD agar plate at 26°C.

See also Figure S5.

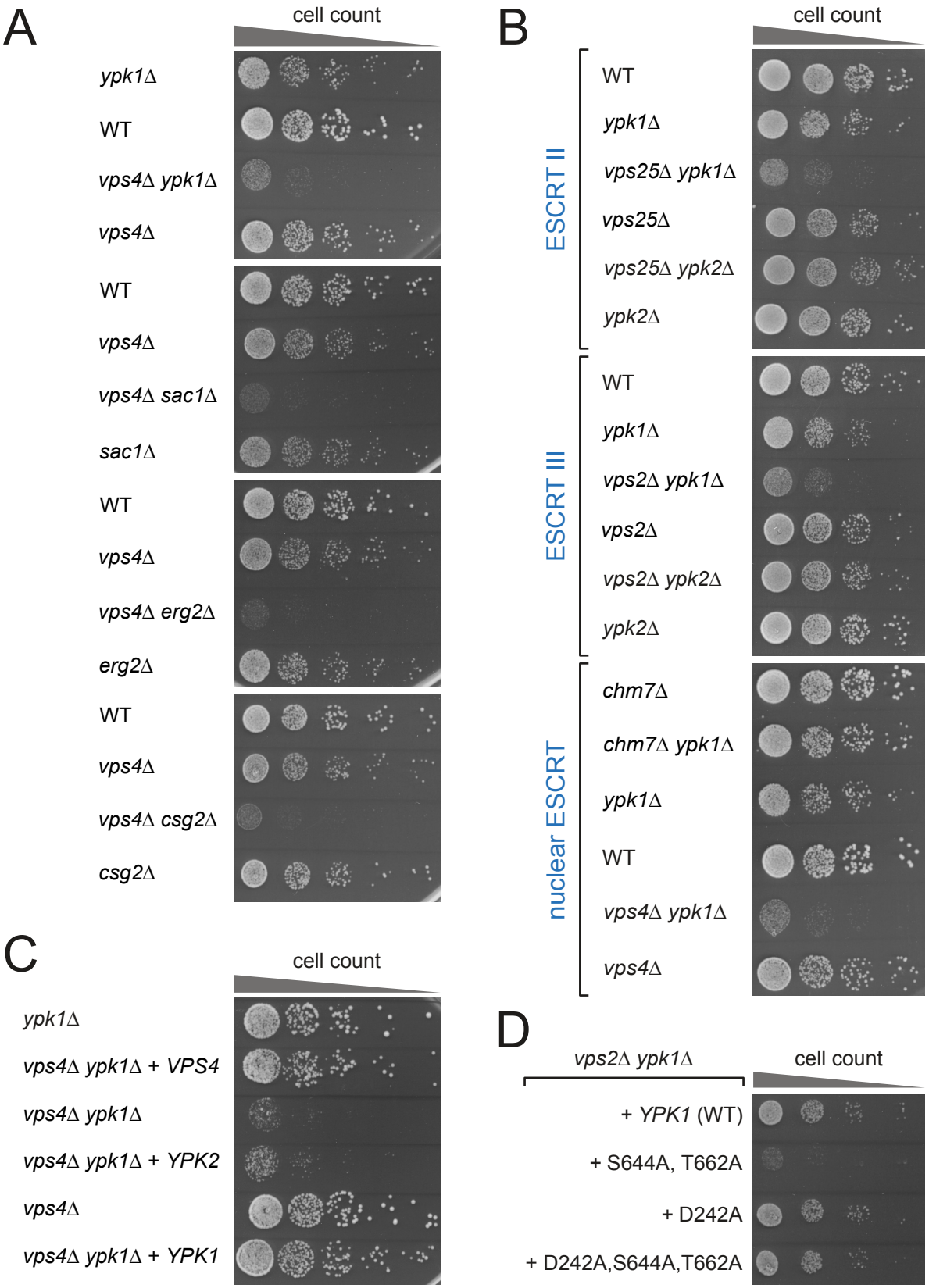

Figure S1 - related to Figure 1

Figure S1 - related to Figure 1.

(A, B) Equal amounts of WT cells and indicated single or double mutants in serial dilutions were incubated on auxotrophic selection medium agar plates at 26°C.

(C) Equal amounts of the indicated single or double mutants complemented with the indicated plasmids (or empty vectors for isogenic controls) in serial dilutions were incubated on auxotrophic selection medium agar plates at 26°C.

(D) Equal amounts of *vps2*Δ *ypk1*Δ double mutants expressing the indicated *YPK1* mutant plasmids in serial dilutions were incubated on auxotrophic selection medium agar plates at 26°C.

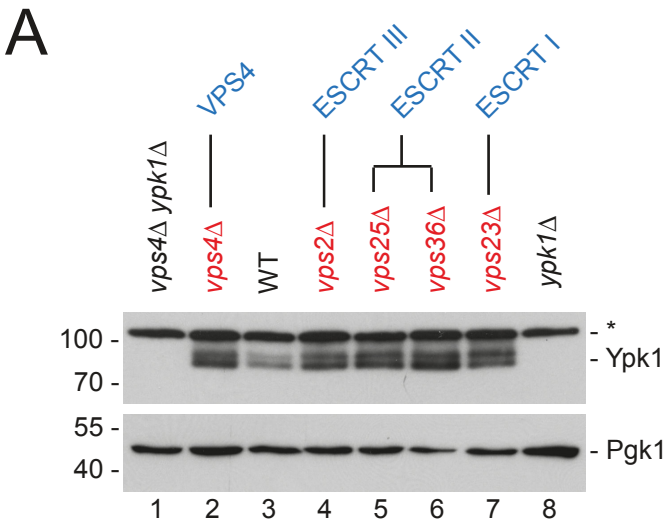

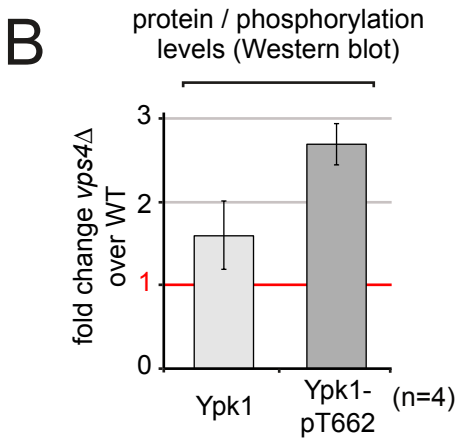

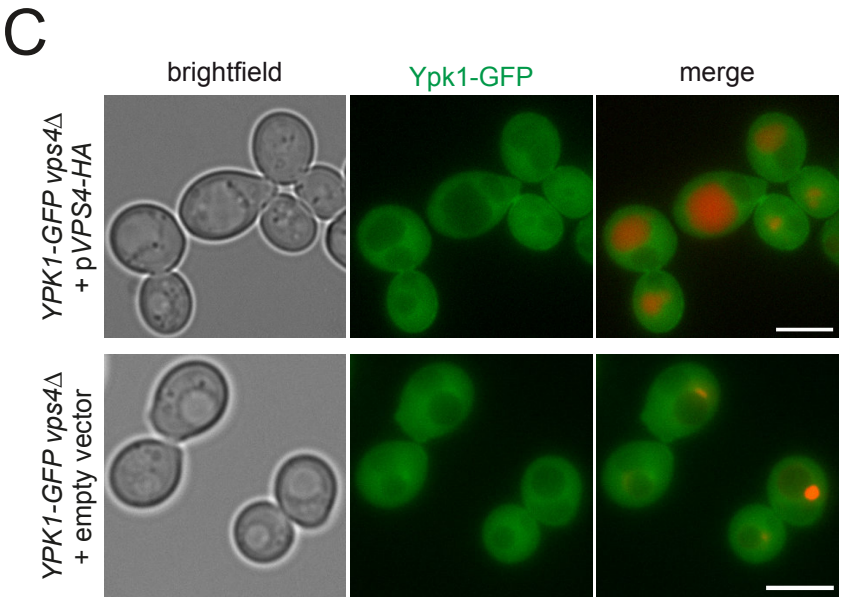

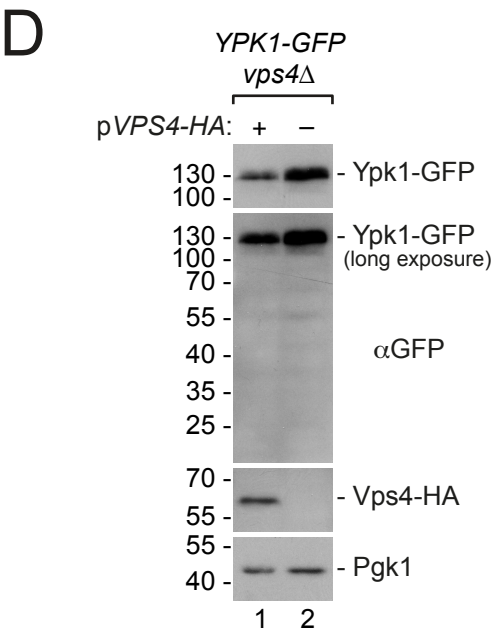

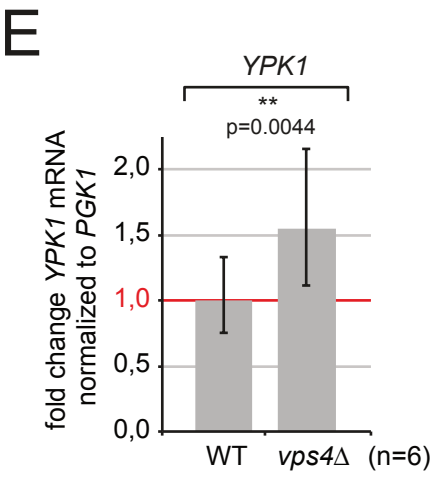

Figure S3 - related to Figure 3

Figure S3 - related to Figure 3.

(A) SDS-PAGE and Western blot analysis with the indicated antibodies of total yeast lysates from WT and the indicated mutants.

(B) Densitometric quantification of Ypk1 protein levels and Ypk1 pT662 phosphorylation levels in WT cells and *vps4*Δ mutants from Western blot experiments normalized to Pgk1 loading control. Data are presented as mean fold change in *vps4*Δ cells compared to WT levels ±standard deviation from 4 independent experiments.

(C) Epifluorescence and phase contrast microscopy of living WT and *vps4*Δ cells expressing Ypk1-GFP (green) and the MVB cargo mCherry-CPS (red). Ypk1-GFP does not localize to the vacuole in WT or the class E compartment in ESCRT mutant cells grown under standard conditions. Scale bars 5µm.

(D) SDS-PAGE and Western blot analysis with the indicated antibodies of total yeast lysates from WT and *vps4*Δ cells expressing *YPK1-GFP*. Only full-length Ypk1-GFP protein was observed in WT cells and ESCRT mutants. The typical free GFP fragment at 25 kD, which would be indicative of vacuolar proteolysis, was not detected.

(E) Quantification of *YPK1* mRNA normalized to stable *PGK1* mRNA from WT cells and *vps4*Δ mutants by qPCR (n=6). Data are presented as mean fold change from WT ±standard deviation. Statistical significance was assessed by Student's t-test.

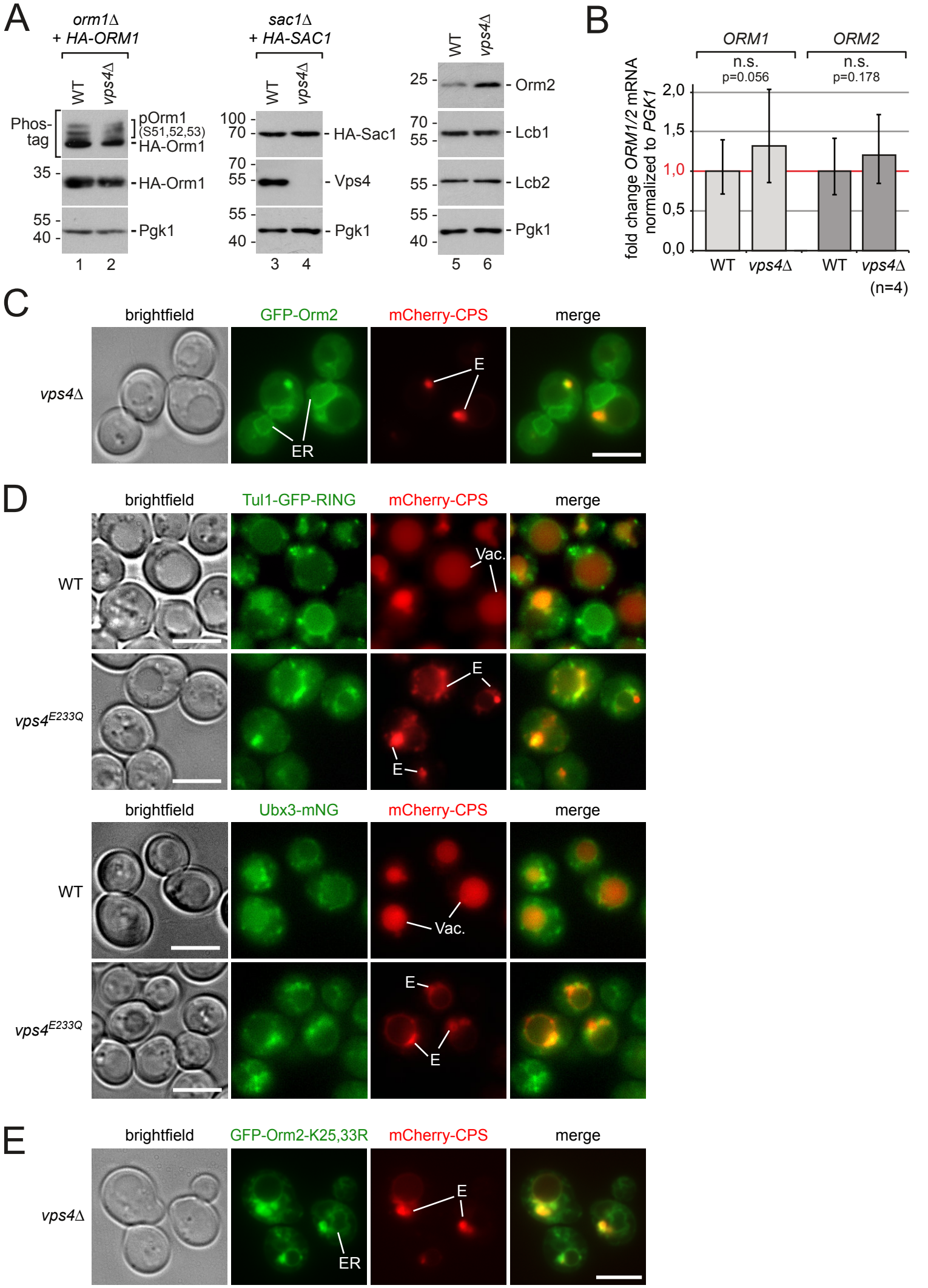

Figure S4 - related to Figure 4

Figure S4 - related to Figure 4.

(A) SDS-PAGE and Western blot analysis with the indicated antibodies of total yeast lysates from the indicated WT or *vps4*Δ strains.

(B) Quantification of *ORM1* and *ORM2* mRNA normalized to stable *PGK1* mRNA from WT cells and *vps4*Δ mutants by qPCR (n=4). Data are presented as mean fold change from WT ±standard deviation. Statistical significance was assessed by Student's t-test.

(C) Epifluorescence and phase contrast microscopy of living *vps4*Δ *(orm2*Δ*)* cells expressing GFP-Orm2 (green) and mCherry-CPS (red). ER, endoplasmic reticulum; E, class E compartment.

(D) Epifluorescence and phase contrast microscopy of living *tul1*Δ cells expressing *TUL1-GFP-RING* (green) or WT cells expressing Ubx3-mNeonGreen (green) and mCherry-CPS (red), and either dominant-negative *vps4*E233Q or empty plasmid as indicated. Vac, vacuole; E, class E compartment. Scale bars 5µm.

(E) Epifluorescence and phase contrast microscopy of living *vps4*Δ *(orm2*Δ*)* cells expressing GFP-Orm2-K25,33R (green) and mCherry-CPS (red). ER, endoplasmic reticulum; E, class E compartment.

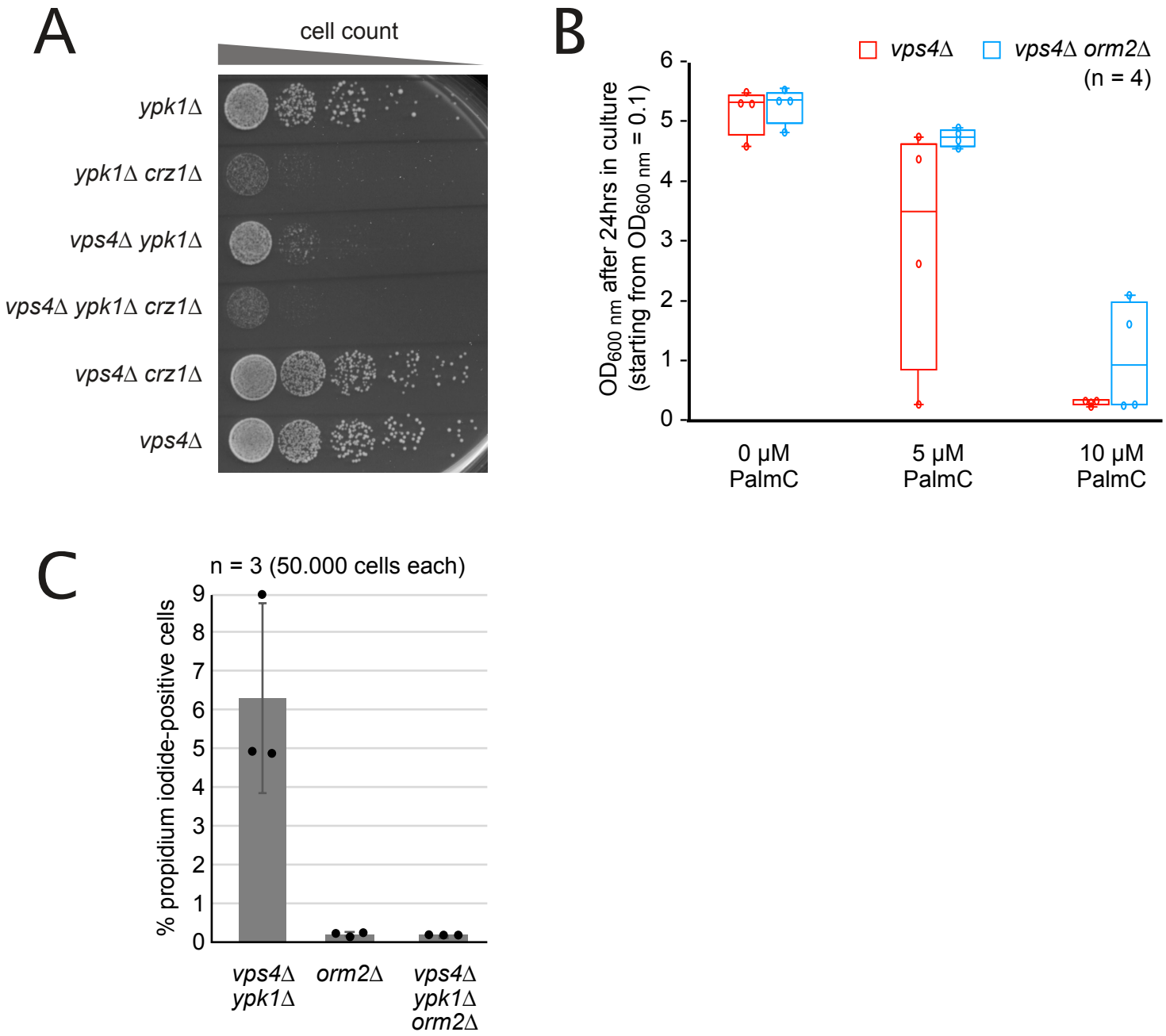

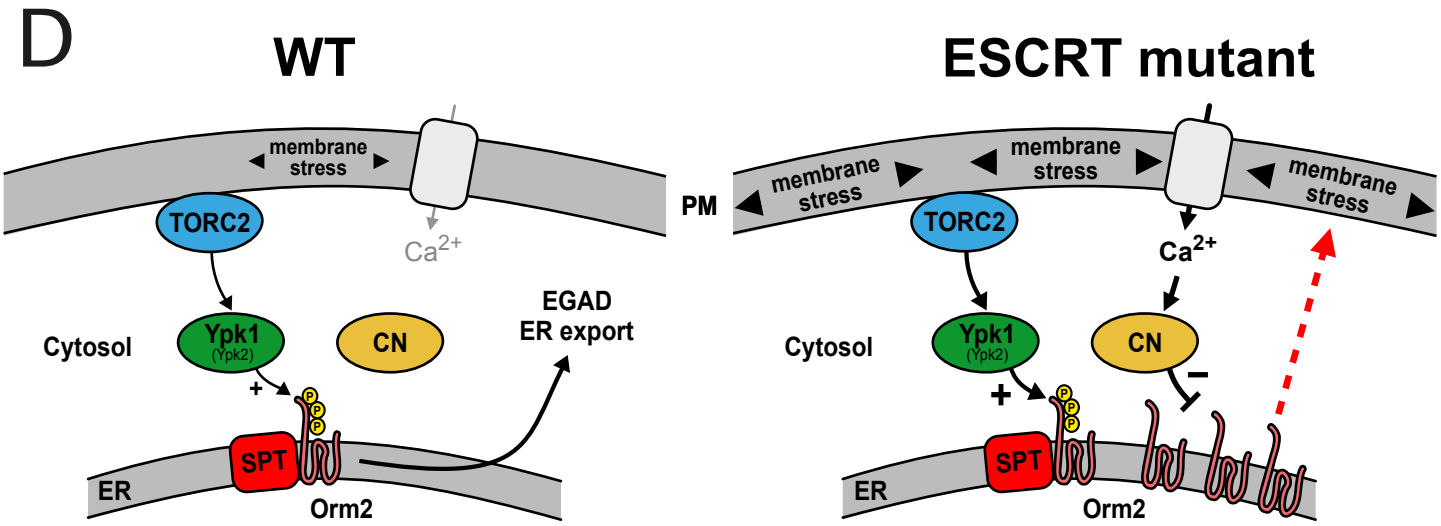

Figure S5 - related to Figure 5

Figure S5 - related to Figure 5.

(A) Equal amounts of the indicated single, double or triple mutants in serial dilutions were incubated on a YPD agar plate at 26°C.

(B) Growth of *vps4*Δ and *vps4*Δ *orm2*Δ cells in auxotrophic selection medium in presence of the indicated PalmC concentrations. Cells were inoculated to OD_{600nm} = 0.1 and grown for 24 hours in 4 independent experiments. The circles indicate the individual measurements.

(C) The indicated strains were grown into mid-log phase in YPD medium and stained with propidium iodide for 10 minutes and analyzed by fluorescence activated cell sorting. Data are presented as mean ±standard deviation from 3 independent experiments. The data for the *vps4*Δ *ypk1*Δ strain is the same as in Fig. 2E and was plotted again for comparison.

(D) Model for the post-translational regulation of Orm2 protein levels in WT cells and its deregulation in ESCRT mutants. PM, plasma membrane; ER, endoplasmic reticulum; TORC2, target of rapamycin complex 2; CN, calcineurin; SPT, serine-palmitoyl-coenzyme A transferase.

Supporting information for

"Multiple roles for the ESCRT machinery in maintaining plasma membrane homeostasis"

Oliver Schmidt[1*], Yannick Weyer[1], Simon Sprenger[1], Michael A. Widerin[1], Sebastian Eising[2], Verena Baumann[1,3], Mihaela Angelova[4], Robbie Loewith[5], Christopher J. Stefan[6], Michael W. Hess[7], Florian Fröhlich[3], and David Teis[1]

[1] Division of Cell Biology, Biocenter, Medical University of Innsbruck, Austria

[2] Department of Biology/Chemistry, University of Osnabrück, Germany

[3] current address: Max Perutz Labs, University of Vienna, Austria

[4] Cancer Evolution and Genome Instability Laboratory, Francis Crick Institute, London, UK

[5] Department of Molecular Biology, University of Geneva, Switzerland

[6] MRC Laboratory for Molecular Cell Biology, University College London, London, UK

[7] Institute for Histology and Embryology, Medical University of Innsbruck, Austria

*Corresponding author:
Dr. Oliver Schmidt
Medical University of Innsbruck, Biocenter, Division Cell Biology
Innrain 80/82, CCB Building
A-6020, Innsbruck, Austria

oliver.schmidt@i-med.ac.at
phone: +43 512 9003 70191
fax: +43 512 9003 73100

content:

- Tables S1 and S2
- Figures S1 and S3-S5

Table S1: Gene ontology term 'molecular processes' enrichment analysis

GOID	GO term	Frequency	Genome Frequency	adj. p-value	enrichment	Gene(s)
GO:0042592	**homeostatic process**	**15 out of 119 genes, 12.6%**	**276 of 6433 genes, 4.3%**	**4,85E-03**	**2,94**	**CSG2,VMA2,PER1,VMA1,NHX1,VMA3,PMR1,VMA7, VMA10,ICE2,VPS53,VMA5,RAD50,PHO80,VMA4**
GO:0006629	**lipid metabolic process**	**15 out of 119 genes, 12.6%**	**296 of 6433 genes, 4.6%**	**5,06E-03**	**2,74**	**DEP1,CSG2,PER1,UME6,CAX4,HTD2,OAR1,YPK1,SAC1, ERG6,ERG5,PAH1,ERG2,ERG24,MCT1**
GO:0006351	**transcription, DNA-templated**	**23 out of 119 genes, 19.3%**	**673 of 6433 genes, 10.5%**	**2,01E-02**	**1,85**	**DEP1,CCR4,RRN10,NHP6B,RXT2,SRB8,HPR1,UME6,HTA1 ,RAD4,SNF6,PFD1,NNT1,SFP1,GIM5,CTK3,MKS1,SIN4, YNL296W,PHO80,THP1,CKA2,SSN3**
GO:0006464	cellular protein modification process	20 out of 119 genes, 16.8%	665 of 6433 genes, 10.3%	7,35E-02	1,63	DEP1,GCV3,PER1,UBX3,NBP2,GDA1,CAX4,TUL1,ELM1, YPK1,LIP2,NNT1,STE11,CTK3,YDJ1,URE2,PHO80,CKA2, SSN3,PPT2
GO:0040007	growth	8 out of 119 genes, 6.7%	165 of 6433 genes, 2.6%	7,35E-02	2,62	RXT2,SEC66,UME6,PDA1,ELM1,STE11,MKS1,SSN3
GO:0006950	response to stress	20 out of 119 genes, 16.8%	672 of 6433 genes, 10.4%	7,35E-02	1,61	DEP1,HTA2,SHP1,TPS1,HPR1,SAC3,ACL4,NBP2,HTA1, EAF1,RAD4,SNF6,YLR235C,IMH1,MMS22,STE11,YDJ1, RAD50,THP1,CKA2
GO:0051276	chromosome organization	17 out of 119 genes, 14.3%	554 of 6433 genes, 8.6%	7,84E-02	1,66	DEP1,TPD3,HTA2,SHP1,NHP6B,RXT2,UBX3,SAC3,UME6, HTA1,EAF1,RAD4,SNF6,NNT1,MMS22,RAD50,THP1
GO:0016192	vesicle-mediated transport	12 out of 119 genes, 10.1%	351 of 6433 genes, 5.5%	8,51E-02	1,85	SLA1,CDC50,UBX3,SWA2,VMA3,GLO3,PMR1,EMP24, VPS53,IMH1,END3,SLA2
GO:0006461	protein complex assembly	10 out of 119 genes, 8.4%	282 of 6433 genes, 4.4%	8,82E-02	1,92	SLA1,PIM1,VMA2,EAF1,VMA21,ICE2,ELM1,GIM5,PKR1, MDM12
GO:0006412	translation	7 out of 119 genes, 5.9%	727 of 6433 genes, 11.3%	8,82E-02	0,52	TPD3,RPS9B,DHH1,RPS24A,RPL34B,MRPL15,CTK3
GO:0005975	carbohydrate metabolic process	7 out of 119 genes, 5.9%	198 of 6433 genes, 3.1%	1,17E-01	1,91	DEP1,SHP1,TPS1,UME6,SNF6,ELM1,EXG1
GO:0061024	membrane organization	9 out of 119 genes, 7.6%	282 of 6433 genes, 4.4%	1,17E-01	1,73	SEC66,CDC50,GLO3,ICE2,YPK1,IMH1,PAH1,PHO80, MDM12
GO:0006259	DNA metabolic process	13 out of 119 genes, 10.9%	453 of 6433 genes, 7.0%	1,17E-01	1,55	DEP1,CCR4,HTA2,HPR1,SAC3,HTA1,EAF1,RAD4,HUR1, SNF6,MMS22,RAD50,THP1
GO:0007010	cytoskeleton organization	8 out of 119 genes, 6.7%	238 of 6433 genes, 3.7%	1,17E-01	1,82	SLA1,SAC6,ICE2,PFD1,ELM1,END3,SRV2,SLA2
GO:0034655	nucleobase-containing compound catabolic process	5 out of 119 genes, 4.2%	146 of 6433 genes, 2.3%	1,39E-01	1,85	CCR4,DHH1,SAC3,THP1,SSN3
GO:0007049	cell cycle	14 out of 119 genes, 11.8%	644 of 6433 genes, 10.0%	1,39E-01	1,18	TPD3,CCR4,SHP1,BUD31,SAC3,UME6,ELM1,MMS22, END3,SLA2,RAD50,YNL296W,PHO80,THP1
GO:0044281	small molecule metabolic process	15 out of 119 genes, 12.6%	675 of 6433 genes, 10.5%	1,39E-01	1,20	DEP1,GCV3,UME6,RNR1,PDA1,HTD2,CYC1,ADO1,ELM1, OAR1,ERG6,ERG5,ERG2,ERG24,MCT1
GO:0071554	cell wall organization or biogenesis	6 out of 119 genes, 5.0%	198 of 6433 genes, 3.1%	1,39E-01	1,64	NBP2,PRS3,EXG1,STE11,END3,SLA2
GO:0006091	generation of precursor metabolites and energy	5 out of 119 genes, 4.2%	154 of 6433 genes, 2.4%	1,39E-01	1,76	SHP1,CYC1,OAR1,YLR294C,PAH1
GO:0007005	mitochondrion organization	2 out of 119 genes, 1.7%	265 of 6433 genes, 4.1%	1,39E-01	0,41	YDJ1,MDM12
GO:0051301	cell division	5 out of 119 genes, 4.2%	127 of 6433 genes, 2%	1,39E-01	2,13	BUD31,ELM1,END3,SLA2,THP1
GO:0000003	reproduction	12 out of 119 genes, 10.1%	467 of 6433 genes, 7.3%	1,39E-01	1,39	SHP1,RXT2,UME6,ELM1,YPK1,MMS22,STE11,END3,SLA2, RAD50,YNL296W,CKA2
GO:0042254	ribosome biogenesis	5 out of 119 genes, 4.2%	416 of 6433 genes, 6.5%	1,45E-01	0,65	RPS9B,SAC3,RPS24A,SNF6,DBP7
GO:0006913	nucleocytoplasmic transport	5 out of 119 genes, 4.2%	180 of 6433 genes, 2.8%	1,72E-01	1,50	HPR1,SAC3,YDJ1,URE2,THP1
GO:0006397	mRNA processing	4 out of 119 genes, 3.4%	170 of 6433 genes, 2.6%	2,09E-01	1,27	BUD31,HPR1,SAC3,THP1
GO:0030154	cell differentiation	4 out of 119 genes, 3.4%	160 of 6433 genes, 2.5%	2,09E-01	1,35	SHP1,END3,YNL296W,CKA2
GO:0007165	signal transduction	5 out of 119 genes, 4.2%	240 of 6433 genes, 3.7%	2,09E-01	1,13	NBP2,STE11,MKS1,SRV2,PHO80
GO:0055085	transmembrane transport	3 out of 119 genes, 2.5%	234 of 6433 genes, 3.6%	2,09E-01	0,69	VMA2,SEC66,NHX1
GO:0048856	anatomical structure development	4 out of 119 genes, 3.4%	160 of 6433 genes, 2.5%	2,09E-01	1,35	SHP1,ELM1,END3,YNL296W
GO:0006605	protein targeting	5 out of 119 genes, 4.2%	307 of 6433 genes, 4.8%	2,09E-01	0,88	SEC66,VMA3,ICE2,YDJ1,URE2
GO:0007059	chromosome segregation	3 out of 119 genes, 2.5%	203 of 6433 genes, 3.2%	2,34E-01	0,80	TPD3,SHP1,MMS22
GO:0007034	vacuolar transport	2 out of 119 genes, 1.7%	168 of 6433 genes, 2.6%	2,34E-01	0,64	VMA3,VPS53
GO:0048646	anatomical structure formation involved in morphogenesis	3 out of 119 genes, 2.5%	137 of 6433 genes, 2.1%	2,34E-01	1,18	SHP1,END3,YNL296W
GO:0006790	sulfur compound metabolic process	2 out of 119 genes, 1.7%	122 of 6433 genes, 1.9%	2,71E-01	0,89	PDA1,MET10
GO:0006457	protein folding	2 out of 119 genes, 1.7%	95 of 6433 genes, 1.5%	2,71E-01	1,14	PFD1,YDJ1

Table S2: Yeast strains, plasmids and reagents

Antibodies	SOURCE	IDENTIFIER
Goat anti mouse IgG-Peroxidase	Sigma	Cat. # A4416; RRID:AB_258167
Goat anti rabbit IgG-Peroxidase	Sigma	Cat. # A0545; RRID:AB_257896
Rabbit anti goat IgG-Peroxidase	Sigma	Cat. # A5420; RRID:AB_258242
Mouse monoclonal anti PGK1 (22C5D8)	Invitrogen	Cat. # 459250; RRID:AB_2532235
Mouse monoclonal anti GFP (IgG1K, clones 7.1 and 13.1)	Roche Diagnostics	Cat. # 11814460001; RRID:AB_390913
Goat anti-GFP polyclonal	Rockland	Cat. # 600-101-215; RRID:AB_218182
Rabbit anti goat Fab' 1.4 nm NANOGOLD™	Nanoprobes	Cat. # 2004
Mouse monoclonal anti FLAG M2	Sigma	Cat. # F3165; RRID:AB_259529
Mouse monoclonal anti HA (12CA5)	Abcam	Homemade hybridoma supernatant, lot 20081201
Mouse monoclonal anti ubiquitin (P4D1)	Santa Cruz	Cat. # sc-8017; RRID:AB_628423
Mouse monoclonal anti Ypk1 phospho-T662	Gift from Robbie Loewith	(Berchtold et al., 2012)
Goat polyclonal anti-Ypk1	Santa Cruz	Cat. # yl15; RRID:AB_793265
Rabbit polyclonal anti-Orm2, generated against N-terminal peptide MIDRTKNESPAFEESPLTP	Gift from Howard Riezman	This study
Rabbit polyclonal anti-Lcb1	Gift from Teresa Dunn	(Gable, Slife et al., 2000)
Rabbit polyclonal anti-Lcb2	Gift from Teresa Dunn	(Gable et al., 2000)
Rabbit polyclonal anti-Tul1	Gift from Peter Espenshade	(Tong et al., 2014)
Rabbit polyclonal anti-Ubx3	Gift from Peter Espenshade	(Tong et al., 2014)
Rabbit polyclonal anti-Dsc2	Gift from Peter Espenshade	(Tong et al., 2014)
Rabbit polyclonal anti-Dsc3	Gift from Peter Espenshade	(Tong et al., 2014)
Rabbit polyclonal anti-Vps4	Gift from Scott Emr	(Babst et al., 1998)
Chemicals, Peptides, and Recombinant Proteins	**SOURCE**	**IDENTIFIER**
[3H]-L-serine	Hartmann analytics	Cat. # MT910
anti-Flag magnetic beads M2	Sigma	Cat. # M8823; RRID:AB_2637089
3xFLAG peptide	Sigma	Cat. # F4799
Phos-tag acrylamide	Wako	Cat. # 304-93521
Cycloheximide	Sigma	Cat. # C7698
Myriocin	Sigma	Cat. # M1177-5MG
Rapamycin	LC Laboratories	Cat. # R-5000
Palmitoyl carnitine	Sigma	Cat. # 91503-10MG
Propidium iodide	Sigma	Cat. # 81845
FK-506	Sigma	Cat. # E3889
Ethylene glycol-bis(2-aminoethylether)-N,N,N,N′ -tetraacetic acid (EGTA)	Sigma	Cat. # 3779

Table S2: Yeast strains, plasmids and reagents (continued)

Commercial Assays	**SOURCE**	**IDENTIFIER**
TAQman gene expression assay for ORM1	Thermo Scientific	Cat. # Sc04125000_s1
TAQman gene expression assay for ORM2	Thermo Scientific	Cat. # Sc04149509_s1
TAQman gene expression assay for YPK1	Thermo Scientific	Cat. # Sc04141261_s1
TAQman gene expression assay for PGK1	Thermo Scientific	Cat. # Sc04104844_s1
RNeasy Mini kit	Qiagen	Cat. # 74104
Revert Aid First strand cDNA synthesis kit	Thermo	Cat. # K1622

Yeast strains:	**SOURCE**	**IDENTIFIER**
SEY6210 wildtype (*MATalpha leu2-3, 112 ura3-52 his3-200 trp1-901 lys2-801 suc2-9)*	(Robinson, Klionsky et al., 1988)	SEY6210
SEY6210.1 wildtype (*MATa leu2-3, 112 ura3-52 his3-200 trp1-901 lys2-801 suc2-9)*	(Robinson et al., 1988)	SEY6210.1
SEY6210 *vps4::TRP1*	(Babst et al., 1997)	MBY3
SEY6210.1 *vps4::TRP1*	(Babst et al., 1997)	MBY4
SEY6210.1 *vps23::HIS3*	(Babst et al., 2000)	MBY23
SEY6210.1 *vps36::HIS3*	(Babst et al., 2000)	MBY13
SEY6210.1 *vps2::HIS3*	this study, (Babst et al., 2002a)	DTY521
SEY6210.1 *vps25::HIS3*	this study, (Babst et al., 2002b)	OSY396
SEY6210.1 *tul1::HIS3*	(Schmidt et al., 2019)	SSY17
SEY6210.1 *orm1::HIS3*	(Schmidt et al., 2019)	OSY510
SEY6210 *orm2::TRP1*	(Schmidt et al., 2019)	YSC580
SEY6210.1 *orm2::TRP1*	(Schmidt et al., 2019)	OSY774
SEY6210.1 *orm2::TRP1 tul1::HIS3*	(Schmidt et al., 2019)	YWY027
SEY6210.1 *vps4::TRP1 orm2::TRP1*	(Schmidt et al., 2019)	VBY51
SEY6210.1 *vps4::TRP1 tul1::HIS3 orm2::TRP1*	(Schmidt et al., 2019)	YWY029
SEY6210.1 *orm2::TRP1 ypk1::HIS3*	this study	VBY61
SEY6210.1 *orm2::TRP1 ypk1::HIS3 vps4::TRP1*	this study	VBY60
SEY6210.1 *orm1::HIS3 vps4::TRP1*	this study	OSY520
SEY6210.1 *orm1::HIS3 ypk1::HIS3 vps4::TRP1*	this study	OSY492
SEY6210.1 *ypk1::HIS3*	this study	MMY059
SEY6210.1 *ypk1::HIS3 vps4::TRP1*	this study	OSY323
SEY6210.1 *sac1::HIS3*	this study	OSY566
SEY6210.1 *sac1::HIS3 vps4::TRP1*	this study	OSY570
SEY6210.1 *csg2::HIS3*	this study	OSY529
SEY6210.1 *csg2::HIS3 vps4::TRP1*	this study	OSY531
SEY6210.1 *erg2::HIS3*	this study	OSY568
SEY6210.1 *erg2::HIS3 vps4::TRP1*	this study	OSY572
SEY6210.1 *ypk2::HIS3*	this study	OSY397
SEY6210.1 *ypk2::HIS3 vps25::HIS3*	this study	OSY398
SEY6210.1 *ypk1::HIS3 vps25::HIS3*	this study	OSY393
SEY6210.1 *ypk2::HIS3 vps2::HIS3*	this study	OSY401
SEY6210.1 *ypk1::HIS3 vps2::HIS3*	this study	OSY394
SEY6210 *ypk1::HIS3*	this study	OSY402
SEY6210.1 *chm7::TRP1*	this study	OSY577
SEY6210.1 *chm7::TRP1 ypk1::HIS3*	this study	OSY579
SEY6210.1 *YPK1-GFP::HIS3 vps4::TRP1*	this study	MMY075

Table S2: Yeast strains, plasmids and reagents (continued)

TB50xSEY *vps4::TRP1 tor1-1 avo3Δ1274-1430::hphMX6, Mat.A*	this study, (Gaubitz et al., 2015)	OSY486
TB50xSEY *vps4::TRP1 tor1-1, Mat.A*	this study, (Gaubitz et al., 2015)	OSY490
SEY6210.1 *orm2::TRP1 vps25::HIS3*	this study	YWY016
SEY6210 *UBX3-mNeonGreen::TRP1*	this study, (Yang et al., 2018)	MWY218
SEY6210.1 *cnb1::HIS3*	this study	OSY274
SEY6210.1 *vps4::TRP1 cnb1::HIS3*	this study	OSY291
SEY6210 *cnb1::HIS3 ypk1::HIS3*	this study	OSY426
SEY6210.1 *vps4::TRP1 cnb1::HIS3 ypk1::HIS3*	this study	OSY427
SEY6210.1 *vps4::TRP1 crz1::HIS3*	this study	OSY466
SEY6210 *crz1::HIS3 ypk1::HIS3*	this study	OSY499
SEY6210.1 *vps4::TRP1 crz1::HIS3 ypk1::HIS3*	this study	OSY497
Primer for gene knock out / knock in	**Used for strain:**	**Primer name:**
GTTCCTCTCATATCAACAAACATTAATACAGTTCCTGAAAC GGATCCCCGGGTTAATTAA	OSY323	YPK1_KO_F
CATCATTCCTGAACTTGAGGTGGCATCATTGGGTGTCCCTG AATTCGAGCTCGTTTAAAC	OSY323	YPK1_KO_R
TGGGTCAAATTATCGCGTATACAAATATACATATAGTAACC GGATCCCCGGGTTAATTAA	OSY397	YPK2_KO_F
TAAAATAGTAGAGTTAGAGGTGATAGGGAAGGGAAGAGTAG AATTCGAGCTCGTTTAAAC	OSY397	YPK2_KO_R
CACCACCAAAGCCAGCCAAATAGTATCTCACTGTATCTGAC GGATCCCCGGGTTAATTAA	OSY577	CHM7_KO_F
CCCACTTTAACACTAGCAATTCGAAGGTCATTTTCTGTGAT GCGAATTCGAGCTCGTTTAAAC	OSY577	CHM7_KO_R2
TCGCTCAATCAAACTAAGACTAGCCCAGACCATTATAGCCC GGATCCCCGGGTTAATTAA	OSY568	ERG2_KO_F
GGACTACCGCATGACTGATTTCGTGAGGTCGGGCAGCTTAG AATTCGAGCTCGTTTAAAC	OSY568	ERG2_KO_R
GCTGGTGAGTTAGCACGATAACAAACAAAGATACAGCGTCC GGATCCCCGGGTTAATTAA	OSY529	CSG2-KO-F
CAAGAATGGGTCAGAAAGTTCACCCGTGTTAGGGTTGACGG AATTCGAGCTCGTTTAAAC	OSY529	CSG2-KO-R
TTTAGTCTCGATTGGAAGTTTCGTCAGACAGTACAAGGAAG CGGATCCCCGGGTTAATTAA	OSY466	CRZ1_KO_F
AAAAAAAAATTCCTATTCAAAGCTTAAAAAAACAAAAATAA GAATTCGAGCTCGTTTAAAC	OSY466	CRZ1_KO_R
CAGTAACGATAATATTTATATACACGTATATTTTCTCGTCT AGATCGGATCCCCGGGTTAATTAA	OSY566	SAC1_KO_F2
CAGCCCAGTATATTGGCACAGATCCTCTTGTCTGTAAGAAG GAGGAATTCGAGCTCGTTTAAAC	OSY566	SAC1_KO_R2
ATGGTGATCAGAATCCATAGAAGCATTTTTATTTCTTAAAC GGATCCCCGGGTTAATTAA	OSY274	CNB1_KO_F
AAATCCACGTCCCCACTATTATCAGCATCGAAAACCTCCAG AATTCGAGCTCGTTTAAAC	OSY274	CNB1_KO_R
Primer for plasmid cloning	**Used for plasmid(s):**	**Primer name:**
gcgGGATCCACTTCCTGAACCTTTGTATAGTTCATCC	pOS218	GFP-Orm2-BamHI-R
cgcaacgttGCTGACGTCTTCTTGAAACCCGTC	pVB01	YPK1_HindIII_F
gcgctcgagGGATCTCGGAAGGGTAAGAGAGG	pVB01	YPK1_XhoI_R
GGTTTCAATAAGATATCTACCTTTGCTGTGACAAGGAAATT ACCTTATTTAAAG	pOS096, pOS097	Ypk1_D242A_F
CTTTAAATAAGGTAATTTCCTTGTCACAGCAAAGGTAGATA TCTTATTGAAACC	pOS096, pOS097	Ypk1_D242A_R
GATCgtcgacGCTGAAGAATACTTGAAGCC	pVB03	SalI_YPK2_fw
CATGactagtCTTCGCTTTGACATCCGC	pVB03	SpeI_YPK2_rev

Table S2: Yeast strains, plasmids and reagents (continued)

gcgTCTAGAGTTTATGTATGTGTTTTTTGTAGTTATAGATTTAAGC	pOS246	Prom-TPI1_XbaI_R
cgcGAGCTCGTACTGTCATCATCGTTTGC	pYW036	TUL1-SacI-F
gcgACTAGTGGAGTTGGAGCGATTTAG	pYW036	TUL1-SpeI-R
CGAGTATATATCGGAGCATGGTAGTAAAGGAGAAGAACTTTTCACTGG	pYW036	TUL1-pH-RING-F1
CCAGTGAAAAGTTCTTCTCCTTTACTACCATGCTCCGATATATACTCG	pYW036	TUL1-pH-RING-R1
GGCATGGATGAACTATACAAAGGTGGAACTGCTGAACATACC	pYW036	TUL1-pH-RING-F2
GGTATGTTCAGCAGTTCCACCTTTGTATAGTTCATCCATGCC	pYW036	TUL1-pH-RING-R2
Plasmids	**SOURCE**	**IDENTIFIER**
empty centromer vector *HIS3*	(Sikorski & Hieter, 1989)	pRS413
empty centromer vector *TRP1*	(Sikorski & Hieter, 1989)	pRS414
empty centromer vector *LEU2*	(Sikorski & Hieter, 1989)	pRS415
empty centromer vector *URA3*	(Sikorski & Hieter, 1989)	pRS416
pRS415 - *VPS4* (endogenous 5' and 3')	(Müller et al., 2015)	pOS014
pRS416 - *VPS4* (endogenous 5' and 3')	(Müller et al., 2015)	pMM22
pRS415 - *VPS4-3xHA* (endogenous 5' and 3')	(Adell et al., 2014)	pOS063
pRS413 - *VPS4-3xHA* (endogenous 5' and 3')	(Adell et al., 2014)	pDT74
pRS416 - *3xFLAG-ORM2* (endogenous 5' and 3')	(Schmidt et al., 2019)	pOS129
pRS415 - *HA-SAC1* (endogenous 5' and 3')	(Schmidt et al., 2019)	pOS166
pRS415 - *GFP-ORM2* (endogenous 5' and 3')	(Schmidt et al., 2019)	pOS173
pRS416 - *GFP-ORM2* (endogenous 5' and 3') (BamHI site)	this study	pOS218
pRS416 - *ORM2* (endogenous 5' and 3')	(Schmidt et al., 2019)	pVB17
pRS416 - *3xFLAG-ORM2*^{S46A,S47A,S48A} (endogenous 5' and 3')	(Schmidt et al., 2019)	pYW001
pRS416 - *3xFLAG-ORM2*^{S46D,S47D,S48D} (endogenous 5' and 3')	(Schmidt et al., 2019)	pYW002
pRS416 - *GFP-ORM2* (endogenous 5' and 3')	(Schmidt et al., 2019)	pYW006
pRS416 - *GFP-ORM2*^{K25R,K33R} (endogenous 5' and 3')	(Schmidt et al., 2019)	pYW028
pRS415 - *VPS4-3xHA-eGFP* (endogenous 3' and 5')	(Adell et al., 2017)	pSS37
pRS415 - *P*^{TDH3}*-mCherry-CPS1(2-270)*	(Adell et al., 2014)	pC29
pRS416 - *P*^{TDH3}*-mCherry-CPS1*	(Adell et al., 2014)	pC6
pRS414 - *P*^{TDH3}*-mCherry-CPS1(2-270)*	this study	pMM29
pRS415 - *P*^{TPI1}*-mCherry-CPS1*	this study	pOS246
pRS416 - *YPK1* (endogenous 5' and 3')	this study	pVB01
pRS416 - *YPK2* (endogenous 5' and 3')	this study	pVB03
pRS415 - *YPK1-13xmyc* (endogenous 5' and 3')	this study, Courtesy from C. Stefan	pOS109
pRS415 - *YPK1-13xmyc T504A* (endogenous 5' and 3')	this study, Courtesy from C. Stefan	pOS110
pRS415 - *YPK1-13xmyc D242A* (endogenous 5' and 3')	this study	pOS096
pRS415 - *YPK1-13xmyc S644A T662A* (endogenous 5' and 3')	this study, Courtesy from C. Stefan	pOS111
pRS415 - *YPK1-13xmyc S644A T662A D242A* (endogenous 5' and 3')	this study	pOS097
pRS415 - *P*^{ADH1}*-GFP-SAC1*	this study, Courtesy from C. Stefan	pOS229
pRS415 - *SNF7-LAP-eGFP* (endogenous 5' and 3')	(Adell et al., 2017)	pSM35
pRS416 - *3xHA-ORM1* (endogenous 5' and 3')	(Schmidt et al., 2019)	pOS127

Table S2: Yeast strains, plasmids and reagents (continued)

pRS415 - *TUL1-GFP-RING* (endogenous 5' and 3')	this study	pYW036
pRS415 - *VPS4*-E233Q	(Adell et al., 2014)	pOS015
pRS416 - *VPS4*-E233Q	(Müller et al., 2015)	pDT84
Software and Algorithms	**SOURCE**	**IDENTIFIER**
Photoshop CS5	Adobe	Version 12.0.4x64; RRID:SCR_014199
Illustrator CS5.1	Adobe	Version 15.1.0; RRID:SCR_010279
Affinity Photo	Serif	Version 1.7.3 RRID:SCR_016951
Affinity Designer	Serif	Version 1.7.3 RRID:SCR_016952
Excel for Mac	Microsoft	Version 16.16.2; RRID:SCR_016137
ImageJ2	(Rueden et al., 2017)	Version 2.0.0-rc49/1.51h; RRID:SCR_003070
Fiji	(Schinderlin et al., 2012)	Version 1.0
Visi View	Visitron	Version 2.1.4
Attune™ NxT software	Life Technologies	v. 3.1.1243.0